AIAA 2003-1130

Hypersonic Stability and Transition Experiments on Blunt Cones and a Generic Scramjet Forebody

Steven P. Schneider, Shin Matsumura, Shann Rufer,
Craig Skoch, and Erick Swanson
Purdue University
West Lafayette, IN 47907-1282

This version slightly modified from original version to plot only every 40th point in figures 11,18,19, and 27. This shortens the file from 14MB to 3MB, and the plots look almost the same. S.P. Schneider 15 Jan. 2003

41st Aerospace Sciences Meeting & Exhibit
6–9 January 2003
Reno, Nevada

Hypersonic Stability and Transition Experiments on Blunt Cones and a Generic Scramjet Forebody

Steven P. Schneider*, Shin Matsumura†, Shann Rufer‡, Craig Skoch§, and Erick Swanson¶
School of Aeronautics and Astronautics
Purdue University
West Lafayette, IN 47907-1282

Abstract

Purdue University continues to develop a 9.5-inch Mach-6 Ludwieg tube, which presently operates with quiet flow only at low Reynolds number. Efforts towards achieving high quiet Reynolds numbers are reported. Measurements of stability and transition are also being carried out, using the existing conventional-noise Mach-6 flow. Model geometries include blunt round cones at zero and non-zero angle of attack, and the Hyper2000 forebody, which is generic for the Hyper-X class of airbreathing cruise vehicles. The transition literature for these cases is reviewed. Stationary streamwise-vortex instabilities are induced on the Hyper2000 using small roughness elements. Their growth is measured with temperature-sensitive paints. Temperature-paints measurements on a sharp cone at angle of attack show preliminary indications of the stationary crossflow vortices. Finally, a preliminary hot-wire profile was obtained on a blunt cone in a single tunnel run using a newly automated traverse.

Hypersonic Transition and Quiet Tunnels

Laminar-turbulent transition in hypersonic boundary layers is important for prediction and control of heat transfer, skin friction, and other boundary layer properties. However, the mechanisms leading to transition are still poorly understood, even in low-noise environments. Applications hindered by this lack of understanding include reusable launch vehicles [1], high-speed interceptor missiles [2], hypersonic cruise vehicles [3], and ballistic reentry vehicles [4].

Many transition experiments have been carried out in conventional ground-testing facilities over the past 50 years. However, these experiments are contaminated by the high levels of noise that radiate from the turbulent boundary layers normally present on the wind tunnel walls [5]. These noise levels, typically 0.5-1% of the mean, are an order of magnitude larger than those observed in flight [6, 7]. These high noise levels can cause transition to occur an order of magnitude earlier than in flight [5, 7]. In addition, the mechanisms of transition operational in small-disturbance environments can be changed or bypassed altogether in high-noise environments; these changes in the mechanisms change the parametric trends in transition [6].

Only in the last two decades have low-noise supersonic wind tunnels been developed [5, 8]. This development has been difficult, since the test-section-wall boundary layers must be kept laminar in order to avoid high levels of eddy-Mach-wave acoustic radiation from the normally-present turbulent boundary layers. A Mach 3.5 tunnel was the first to be successfully developed at NASA Langley [9]. Langley then developed a Mach 6 quiet nozzle [10]. Unfortunately, this nozzle was removed from service due to a space conflict. No hypersonic quiet tunnels are presently operational anywhere in the world.

The general prediction of transition based on simulations of the transition mechanisms is a very complex and difficult problem. There are several known receptivity mechanisms, several different known forms of instability waves, many different parameters that affect the mean flow and therefore modify the stability properties, and many known nonlinear breakdown mechanisms. The parameter space is large. The scramjet-vehicle forebody and

*Associate Professor. Associate Fellow, AIAA.
†Research Assistant. Student Member, AIAA.
‡Research Assistant. Student Member, AIAA.
§Research Assistant. Student Member, AIAA.
¶Research Assistant. Student Member, AIAA.

and the blunt round cone at angle of attack were selected as generic geometries that appear to be representative for vehicles of current interest.

Scramjet Forebodies and Boundary-Layer Transition

Selection of Model Geometry

To improve our ability to simulate the mechanisms of transition, we need to select a model geometry on which to make detailed measurements and computations. In other words, the validation of a transition-prediction code requires 'building-block experiments', in which detailed measurements of the flow physics are made and compared to the simulations [11]. But what geometry should be used? According to Marvin, the test conditions should be representative of flight [11, Fig. 8]. In the past, most such experiments have also used simple geometric shapes, in order to simplify the experiments and simulations, and many would argue that such simple shapes should still be used. At one time, limitations on computational resources required the use of such simple shapes, but current hardware allows the simulation of flow past more complex shapes, so the use of simple shapes is no longer a necessity.

For low speed work on the crossflow instability, Saric selected a specific 3D wing at a specific condition in order to study crossflow waves in isolation, without interaction with TS waves [12]. In this case, the geometry is not simple, but the resulting flow field has a relatively simple transition mechanism, that allows study of transition induced by a single type of wave in isolation. Measurements of this type are clearly needed in high-speed flow, and will be very important to the process of building up validated codes and a clear understanding of the transition processes. In the low-speed case, however, the crossflow instability was already known to be a major mechanism in swept-wing transition. What mechanisms are dominant for representative vehicles at hypersonic speeds? Which mechanisms should be selected for such detailed studies of single wave types?

Since there are many possible mechanisms that could be subjected to detailed study, a large number of such studies might have to be carried out before useful transition-prediction schemes could be developed. The parameter space is large, and at present it is not clear whether any such study would be carried out in a useful region of the parameter space. *The dominant transition mechanisms on representative flight vehicles are not known.* It therefore seems critical to establish a link between designers who work with representative vehicle shapes, and researchers at work on the understanding and simulation of various transition mechanisms. One way to establish this link is through detailed studies of the transition mechanisms on a generic scramjet forebody.

Work on the generic scramjet forebody therefore has three overall objectives:

1. Determine the mechanisms of transition. This will help to guide the direction of future research. It will also help designers in the extrapolation of wind tunnel data.

2. Begin to make detailed measurements of some of these mechanisms, for detailed development and validation of simulations.

3. Determine the effect of tunnel noise on transition on scramjet forebodies, to aid designers in the extrapolation of existing noisy-tunnel data to flight.

For this plan to work, the generic forebody must be representative of a broad range of designs, which will not soon become obsolescent. It was thought best to obtain the geometry from the designers themselves. A number of designers and applied researchers were contacted as part of the geometry-search effort, including Keith Numbers at AFRL, D.R. Komar at NASA Marshall, and Kei Lau and Ed Eiswirth at the Boeing Phantom Works in St. Louis.

The final generic geometry was obtained from the Hyper-X Program Office at NASA Langley, through Charles McClinton. The files are titled `hyper_2000_oml`; the geometry is called the 'Hyper2000'. The geometry is *'representative of the Hyper-X class of vehicles.'* It is unclassified and releasable to the public, an important feature of a geometry that is studied in an academic institution with basic research funding. It appears very similar to the forebody of the Hyper-X, and the centerplane geometry of the forebody is identical [13].

Figure 1 shows a detail of the side view of the forebody. The forebody is flat over the middle of the vehicle. The Hyper-X and the Hyper2000 have two compression corners, of 5.5 and 3 degrees, following an initial wedge with an included angle of 2.5 degrees. The chines (to the sides of the flat part of the lower surface) and the upper surface are very important to establishing the 3D pressure distribution, and any crossflow. The forebody model geometry

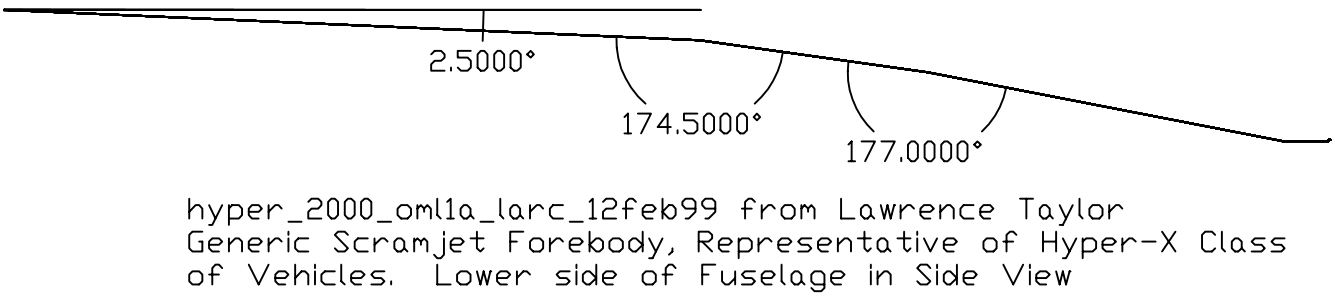

Figure 1: Side View of Hyper2000 Forebody

was obtained by truncating the Hyper2000 near the entrance to the combustor cowl (at the end of the second ramp). The model is very similar to Berry's [13].

Properties of the Flowfield on the Generic Forebody

Scott Berry from NASA Langley has published measurements on the Hyper-X [13, 14]. Taken as a whole, the data suggest the following picture. The flow upstream of the first corner is downstream, with little spanwise crossflow. The laminar boundary layer entering the first corner forms a separation bubble. The bubble affects the flow near the surface, as does the change in spanwise pressure gradient presumably associated with the increased wedge angle downstream of the corner. Crossflow is induced in the boundary layer downstream of the first corner, with *the amount of crossflow that occurs being dependent on the properties of the boundary layer entering the first ramp, downstream of the first corner*. The second corner does not seem to cause any dramatic changes. Since the Mach-6 oilflow seems generally similar to the Mach-10 data, these appear to be generic effects.

These data suggest that the following instability mechanisms should be considered.

1. Second-mode instability in the cold-wall flow at Mach 6 upstream of the first corner (compare Ref. [15]).
2. Shear-layer instabilities in the separated flow at the corner(s).
3. Crossflow instability in the ramp flow.

Görtler instability near the compression corner is also a possibility [16].

Several questions are immediately evident:

1. Can streamwise vortices from the leading edge, any trips, or from shear-layer instabilities, couple into the crossflow instability downstream of the corner, to form a dominant mechanism? This seems particularly likely, since for reattaching shear layers above the separation bubbles that can occur in compression corners, vorticity from the leading edge is known to be a trigger.
2. Can second mode waves generated upstream of the first corner couple into the shear layer instabilities to form the dominant transition mechanism?
3. Do first mode waves have large amplitude upstream of the corner, and how do they interact?

Berry's data also shed light on the difference between Mach 6 and Mach 10, and on some of the tripping questions that will remain issues for the smaller-scale missile designs. Tripping at Mach 10 was much more difficult, as would be expected [17, 18]. Larger trips are required, and transition begins downstream of the trips anyway. Trips that are too large tend to cause streamwise vorticity that convects right into the combustor inlet. At Mach 6, relatively small trips caused transition to occur downstream of the first corner. Larger trips could move transition to the roughness element.

Only one quiet-flow test of a scramjet forebody is reported in the open literature, and the information presented there is very limited [19]. The model was a NASP-like geometry and was tested in the Langley Mach 3.5 quiet tunnel. It had a 0.012-inch radius nose on a 3.6-degree wedge forebody, followed by unspecified compression ramps. Measurements in the region past the first corner showed length transition Reynolds numbers of about 6 million for quiet conditions, and about half that under noisy conditions [19]. Forward of the first corner, on the centerline, transition did not occur under quiet-flow conditions. Transition did occur forward of the first corner off the centerline.

Review of Laminar Compression Corners and Their Effects on Transition

The Hyper2000 geometry selected for study contains a flow feature which is rarely studied in connection with transition. This section therefore reviews compression corners and boundary layer transition.

The compression corner is a classical example of shock/boundary-layer interaction [20, 21, 22, 23, 24, 25]. A shock is generated at the corner and interacts with the incoming boundary layer. Many practical cases involve turbulent incoming boundary layers, so many reviews consider primarily the turbulent case [24]. Stollery reviews the laminar case in two pages [25]. He points out a repeated issue, that *'No real interaction can be genuinely two-dimensional.'* Separation is more likely as the turning angle is increased. Incipient separation for a laminar layer is correlated to

$$M_\infty \alpha_i \simeq 80 \bar{\chi}^{1/2},$$

where

$$\bar{\chi} = M_\infty^3 \left(C/Re_L\right)^{1/2},$$

α_i, the compression angle at incipient separation, is measured in degrees, Re_L is the length Reynolds number of the laminar boundary layer approaching the corner, and C is taken as unity. If $Re_L \simeq 1 \times 10^6$ for our experiments (depending on allowable model size and quiet-flow Reynolds number), then $\bar{\chi} \simeq 0.2$, and $\alpha_i \simeq 6$ degrees. Since the first corner on the Hyper2000 has a 5.5-degree angle, the correlation suggests that laminar separation is marginal, and may or may not occur. Occurrence can probably be controlled by changes in angle of attack. Stollery also points out that *'The detailed patterns described here are crucially dependent on two phenomena which will powerfully influence the whole flow field, namely transition and separation.'*

Delery points out that most 'laminar' interactions are actually transitional, since transition commonly occurs in the shear layer above the separation bubble, which is very sensitive to small disturbances [20]. Since nearly all known studies were carried out in noisy conventional tunnels, substantially different results may be observed in our quiet tunnel. Streamwise vortices are commonly observed in heat-transfer measurements at reattachment; these are presumably generated by an unknown instability in the shear layer [20, 26].

De Luca et al. study these streamwise vortices in detail, using IR imaging, using corner angles of 10-deg. and larger, at Mach 7. De Luca shows that their location can be unambiguously connected to small flaws in the leading edge [27]. De Luca's work is remarkably reminiscent of Saric's work with the triggering of stationary crossflow vortices by small roughness [12], and suggests that careful experiments with small roughness elements should be able to work out the vortex-growth mechanisms. The small roughness elements could be simulated with small streamwise vorticity in computations, for comparison. It should be possible to measure the growth of the vortices using temperature-sensitive paints.

Stollery outlines free-interaction theory, which gives fairly good agreement for the mean properties [25]. Sophisticated triple-deck theory is presented by Cassel et al., but the results were not compared to experiment or theory [28]. Cassel et al. claim to have discovered a new form of instability in the separating boundary layer, but this claim remains to be confirmed by computation or experiment [29]. Inger presents free-interaction theory for prediction of incipient separation, but no flowfield details are presented [30].

Grasso presents 2D computations of a laminar compression corner [31]. Upstream of the corner, laminar computations give fairly good agreement when a fine grid is used. However, agreement is poor downstream, perhaps because transition occurs in the experimental shear layer.

Rudy et al. compute a Mach 14 compression corner using four methods [32]. For laminar incoming flow, with small corner angles that cause little or no separation, 2D computations provide good agreement with surface pressure and heat transfer. For the largest corner angle, the separated region is roughly 50% of L, and a 3D computation must be performed to obtain good agreement. The good agreement obtained in this 1991 work suggest that stability computations are a reasonable next step. This work also suggests that 2D computations are a reasonable place to start.

A number of experimental studies have measured some of the flow details, although nearly all contain only surface measurements. Chpoun et al. measure the surface pressure and heat transfer in a laminar 2D compression corner [33, 34]. At larger angles, the flow reattaches turbulent. For a 10-degree corner at Mach 5 and $Re_L \simeq 1 \times 10^6$, the flow reattaches laminar. This suggests that our geometry will provide a laminar reattachment under quiet-flow conditions.

Simeonides et al. performed both computations and experiments, in 2D, at Mach 6 and 14 [35, 36]. Schlieren images were obtained and surface pressure and temperature were measured. Good agreement is obtained, but not of a quality sufficient for stability

analysis.

Heffner et al. use an axisymmetric geometry for their measurements, to avoid end-effect difficulties [37]. For a 10-degree corner at Mach 5, transition moves from just downstream of the reattachment point, at $Re_L \simeq 0.65 \times 10^6$, to the location of the reattachment point, at $Re_L \simeq 1.0 \times 10^6$. Under quiet flow it is presumably possible to maintain laminar flow well downstream of the corner, at these Reynolds numbers.

Lu et al. measure using corners of 10 and 20 degrees, at Mach 8 and $Re_L = 2.27 \times 10^6$. They attempt to determine the effect of the corners on transition [38]. Although they predicted separation for a 5-7 degree corner, it did not occur. Unfortunately, their shock-tunnel surface pressure measurements did not discriminate well between tunnel noise and turbulent fluctuations.

The authors are aware of three experiments in which flowfield details were measured. Lewis et al. made broadband hot-wire measurements in a 2D Mach-6 10.25-deg. corner, with a laminar incoming boundary layer at $Re_L = 0.068 - 1.0 \times 10^6$ [39]. At $Re_L = 0.15 \times 10^6$, the flow was laminar through reattachment. Hot wire measurements were performed in the separated shear layer, and the RMS fluctuations were obtained. In the corner region, these were sharply peaked in the wall-normal direction. At low Reynolds number, the peak increases slowly in the aft direction, with the location moving towards the wall. At higher Reynolds number, the peak is more broad and the maxima is less well defined, indicating transitional flow.

Kosinov et al. made hot-wire measurements at Mach 2 on a 5-deg. half-angle cone-flare with a 5-deg. compression corner [40]. Separation occured in the corner. The fluctuations in the corner were measured, and controlled perturbations were introduced at 20kHz using a glow perturber set up as a harmonic point source. Oblique first-mode waves were observed to grow at all angles. Low frequency oscillations were observed in the separated region (up to 10kHz), but few details are provided. Kosinov (private communication, March 1999) stated that the length was 150 mm from the nose to the corner, resulting in $Re_L \simeq 1.0 \times 10^6$. Laminar separation occured about 6-7 mm upstream of the corner. In the wall-normal direction, there were two maxima in the fluctuation amplitudes, one at $y/\delta = 0.2 - 0.3$, and one at $y/\delta = 0.5 - 0.6$. The details have not yet been written up for publication due to budget limitations.

Maslov et al. performed the most systematic measurements of transition in the corner, with funding from Aerospatiale [41]. The model was a 7-deg. half-angle cone with a 10-deg. corner at the flare. The measurements were made at Mach 6, with $L = 120$ mm, and $Re_L \simeq 1.4 \times 10^6$. Flowfield measurements were made with hot wires and pitot probes, and surface measurements of the static pressure, heat flux and temperature were obtained. A glow perturber was operated at 40kHz as a harmonic point source. Laminar flow was observed through reattachment, with turbulent flow downstream. *'Low-frequency disturbances (less than 20 kHz) in the separation region increase slowly (by about 1.5 times). Disturbances in the medium-frequency region are neutral. High frequency pulsations (greater than 80kHz) increase strongly (about by a factor of 5).'* Maslov was not yet able to introduce the high frequencies in a controlled way. For controlled disturbances generated at 40kHz with the harmonic point source, the first mode was observed at high wave angles, and the 2nd mode at small wave angles. The conventional tunnel is noisy, so the hot-wire spectra have lots of low frequency noise.

The authors are aware of only two sets of flight measurements in which a compression corner was present. These were made on the flare of a flared cone-cylinder. In the first, it unfortunately appears from the surface heat-transfer data that the boundary layer was turbulent before it arrived at the corner [42]. In the second, transition may occur on the flare at high Mach numbers, but angle-of-attack effects are present, and 3D computations would be required to determine if transition occurs [43].

Finally, the corner separation raises the issue of transition in free shear layers. This topic was reviewed by Demetriades [44], who provides various correlations. Liang and Reshotko worked out a stability analysis for a shear layer between streams at Mach 3 and Mach 8, and compared to other data by Demetriades [45]. King et al. studied transition in a free-shear layer above a cavity, in the Langley quiet tunnel at Mach 3.5 [46]. They showed that quiet flow had almost no effect on the shear-layer transition, presumably because of noise transmitted upstream from the shear-layer reattachment, through the subsonic cavity. It seems possible that end effects or the impinging nozzle shock could also be the explanation. The effect of tunnel noise on the transition mechanisms associated with compression-corner flow remains to be determined.

In summary, various correlations exist for incipient separation in the corner and for the heat transfer and pressure distribution. Three sets of measurements exist for the flowfield properties in the

laminar separating corner. One of these is fairly detailed, and should allow a comparison between the present work and an axisymmetric configuration. A number of computations have also been performed. It appears that work on the transition mechanisms observed in compression-corner flows is a reasonable next step for work in the United States.

Transition on Blunt Cones at Angle of Attack

The blunt cone at small angle of attack is generic for ballistic reentry vehicles, and may also be generic for hypersonic rocket-powered missiles of shorter range. Considerable flight data exists for ballistic RV's, which makes it possible to compare future prediction methods to flight. Although many transition measurements have been made on sharp and blunt cones at zero angle of attack (AOA), and on sharp cones at AOA, there are not many transition measurements on blunt cones at AOA, and there are few stability measurements, even on sharp cones at zero AOA. Real vehicles always have some bluntness, and always have some non-zero AOA. Although modern computational methods allow taking these factors into account, existing experimental data is insufficient for development and validation. The following abbreviated review of the open literature will address effects of small bluntness and small AOA.

Angle-of-Attack Effects on Sharp Cones

DiCristina made measurements on an 8-deg. half-angle sharp cone at AOA and Mach 10 [47]. For a 2-deg. AOA, transition on the leeward ray moved forward by 20%, and was 60% forward at 4-deg. Transition can be very sensitive to small AOA, as has often been shown. However, here transition moved aft very little on the windward ray with AOA. The effect of dynamic motion was secondary, although ablating effects were as important as AOA.

Adams reviewed flow visualization data on sharp cones at angle of attack [48]. These data show striations corresponding to crossflow vortices, which form some distance downstream of the nosetip, and disappear upon the onset of transition. For examples, see Refs. [49] and [50, Fig. 21]. Adams correlated the onset of vortex formation with the crossflow Reynolds number, computed using a 3D boundary-layer code. The angle of the vortices was also correlated using stability theory. Adams provided his code to the present author (private communication, 2002). This work is one of the very few in the existing literature which clearly show a relationship between experimental data and a theoretical transition mechanism.

Fischer measured transition on sharp and blunt cones at angle of attack and Mach 7 [51]. For the nonablating sharp cone, transition moved forward on the leeward ray and aft on the windward ray. For the blunt nonablating cone, transition occured only on the leeward ray, and was aft of the sharp cone case. For a cold-ablating cone with a nonablating tip, longitudinal vortices were observed in the ablated surface, especially at the higher unit Reynolds numbers. These were attributed to a Görtler-type instability aft of the rearward-facing step that formed behind the tip. Ablation lowered the transition Reynolds number by 28 to 35 percent.

Fischer also measured transition on nearly-sharp 2.87-deg. half-angle cones at Mach 21 in the hypersonic helium tunnel at Langley [52]. Transition moved aft on the windward ray and forward on the leeward ray, except for AOA of less than 1 deg., where these trends were reversed. The results reported in Ref. [52] contradict earlier measurements in the same facility that used a pitot tube instead of heat-transfer measurements to detect transition. The complex curve of transition location vs. AOA that is shown in Fischer's Fig. 2 has never been explained.

Mateer measured transition on sharp cones at Mach 7.4 [53]. Reynolds numbers based on edge conditions were computed using the method of characteristics and a boundary layer analysis. For a 5-deg. half-angle cone, length transition Reynolds numbers based on edge conditions (Re_{xe}) increased with AOA on the windward ray, and decreased on the leeward ray. For a 15-deg. half-angle cone, Re_{xe} decreased with AOA on both the windward ray and the leeward ray. Windward-ray transition on several cones in several experiments were correlated using momentum-thickness Reynolds number divided by edge Mach number, plotted against a streamline-spreading parameter. More detail is given in Ref. [54]. Although the title calls the cones 'sharp', the nose radius is not reported. Tabulated data shows that for the 15-deg. cone, transition on the windward ray actually moved forward as the AOA was increased. However, since unit Reynolds number was varied at the same time as AOA, tunnel noise effects corrupt the data, and would be very difficult to separate from AOA effects.

Kendall rolled a 4-deg. half-angle sharp cone at nominally zero AOA, and detected a 10% variation in transition Reynolds number, although the cone was visually free of defects, and no effects of tunnel

nonuniformity were detected [55]. Transition is obviously very sensitive to small asymmetry, although a 10-deg. half-angle cone was much more symmetric.

Stetson measured detailed boundary-layer profiles and laminar instability on a 7-deg. half-angle sharp cone at Mach 8 [56]. After 17 years, this is still one of the most sophisticated experiments carried out on a hypersonic round cone at AOA, although the data is very limited. Profiles were measured on the windward and leeward meridians. Instability-wave amplification was deduced from spectral measurements. The critical Reynolds number for the onset of instability increased on the windward ray and decreased on the leeward ray. First-mode amplification rates decreased on the windward ray, while second-mode amplification was not greatly affected by AOA. Windward-ray transition occured later than in any previous experiments.

Boylan et al. also made measurements of the shock-layer profiles on the leeward ray of a 4-deg. sharp cone at 2.94-deg AOA and Mach 9.82. The results were compared to a viscous-shock-layer computation, which showed limited agreement [57].

Simen et al. made detailed computations for a sharp cone at AOA, at Stetson's conditions [58]. The thin-layer Navier-Stokes equations were used for the mean flow. Computed amplification rates on the leeward ray showed good agreement with Stetson's measurements.

Hanifi et al. computed the stability of flow past a supersonic sharp cone, but based their mean-flow solutions on asymptotic approximations for small AOA [59]. They look at stability on the windward and leeward ray. For AOA of 1 deg. on a 10-deg. half-angle cone, the most unstable 2nd mode wave shifts from 2D to oblique, and the 1st-mode amplification rates change by 40%. Small AOA has a large effect on stability, mostly because the crossflow carries low-momentum fluid around the cone, and changes the boundary-layer profile.

Olsson made detailed measurements of instability on a 7-deg. round cone at AOA and Mach 3 [60]. Away from the sharp tip, similar profiles were observed along the windward and leeward rays. However, the uncalibrated hot-wire data were not reduced beyond plotting profiles. Ref. [61] reports additional measurements on blunt cones including AOA, but again the report gives only raw profiles without analysis. Ref. [62] summarizes the work. At a 1-deg. AOA, the sharp-cone transition moves forward by more than 50% on the leeward ray. The sensitivity to AOA is about half that amount for a 10-mm nose radius.

Doggett et al. made stability measurements on a sharp flared cone at AOA in the Langley Mach-6 quiet tunnel [63]. This is the second existing set of hypersonic stability measurements on a cone at AOA, and the only set carried out under low noise conditions comparable to flight. The boundary-layer on the windward ray was more stable than at zero AOA, and the leeward ray was less stable. Second-mode instability was dominant at zero AOA but was stabilized on the windward ray at AOA. The very high frequency of the dominant instability on the leeward ray was thought to indicate the presence of an instability differing from the normal second mode. Quantitative comparison to computations is difficult since the hot-wire was not calibrated.

Ladoon et al. measured amplification of repeatable instability-wave packets on a Mach-4 cone at AOA [64, 65]. However, the artificially-generated packets grew by factors of only 1.5-3 at the low Reynolds numbers available in the Purdue Mach-4 quiet Ludwieg tube.

Perraud et al. summarize Mach-7 experiments and computations on a 7-deg. half-angle sharp cone at 2-deg. AOA [66]. Transition location varied from 40% of body length on the leeward ray to 76% on the windward ray. Halfway between, transition occured at 61%, and both crossflow and 2nd-mode instabilities had about the same N factor, with the first mode and crossflow modes becoming difficult to distinguish. Stability computations using e^N could predict the general trends, although quantitative agreement was poor, and N was only 1.2 in the small conventional wind tunnel that was used.

Blunt Cones at Zero Angle of Attack

Stetson reported transition measurements on a blunt cone at zero AOA, scaling the reported data with the entropy-layer swallowing length [67]. The swallowing length is the distance downstream where the variations in streamline entropy caused by passage through the curved bow shock are nearly completely swallowed by the boundary layer. Transition that occurs near the swallowing length is delayed compared to a sharp cone, transition that occurs far forward of the swallowing length is dominated by nosetip roughness, and transition that occurs in the middle exhibits lower transition Reynolds numbers than for a sharp cone. For the larger bluntnesses, transition on the frustrum became very sensitive to small roughness on the nosetip, in part due to the large unit Reynolds numbers necessary to achieve transition. The nosetip pits during operation due to blasting by contaminating flowfield particulate,

making repeatable experiments difficult. Stetson believes that the same effect contaminates the large-bluntness data of Muir and Trujillo (see below). The transition delay that occurs near the swallowing length is highly dependent on Mach number as well as bluntness. Ref. [68] reports more details on the sensitivity to nosetip roughness at zero AOA. Ref. [69] also reports additional detail, including the significant effect of placing the cone off the tunnel centerline.

Zanchetta et al. measured transition on a blunt cone at zero AOA in the gun tunnel at Imperial College at Mach 9 [70]. Intermittency was measured using an array of surface thin films. For a large bluntness with a Reynolds number of 1.08×10^6 based on nose radius and freestream conditions, the flow was visualized using liquid crystals. When the nosetip was polished, the flow remained laminar to $Re_s > 3 \times 10^7$. When 50 μm diameter roughness elements were placed on the nosetip, vortex streaks were observed downstream, and transition occured by $Re_s = 4 \times 10^6$. Few details are reported.

Ericsson correlated ground-test and flight data for transition on blunt cones [71]. He also scaled the arclength with the swallowing length, adding a correlation and a comparison to the flight data.

Stability measurements on blunt cones at zero AOA were reviewed in Ref. [72]. All existing measurements fall short of code-validation quality.

Rosenboom et al. computed the mean flow and instabilities of a blunt cone at zero AOA [73]. An e**N analysis shows transition moving monotonically downstream with increasing bluntness, suggesting that receptivity, roughness, or transient growth must come into play to explain the forward movement of transition that occurs at large bluntness. Accurate mean flows are needed for good stability computations; Rosenboom et al. used a thin-layer Navier-Stokes code to account for the nose-bluntness effects.

Bountin et al. measured detailed wave growth on a blunt cone at zero AOA, at Mach 6 [74]. Second-mode instabilities that were measured on a sharp cone were damped when bluntness was added. A perturber was used to generate controlled first and second-mode disturbances. Additional measurements were recently obtained by the same group and are reported in Ref. [75]. The second mode is again damped by bluntness, well downstream of where the entropy layer appears to be swallowed by the boundary layer. However, the second mode is still unstable, and is still most unstable when two-dimensional.

Blunt Cones at Angle of Attack

Stainback made measurements on the windward and leeward rays of a blunt cone with roughness at AOA [76]. The roughness was all downstream of the nosetip. Transition exhibited the usual unit Reynolds number effect, and moved forward on the leeward ray and aft on the windward ray.

Muir and Trujillo measured transition on the windward and leeward rays of sharp and blunt cones at AOA, at Mach 6 [77]. At zero AOA, transition moves aft as bluntness rises from zero, and then moves forward again at large bluntness. For very large bluntness, transition moved aft during the run as the model heated up. For small bluntness, transition is leeside forward and windside aft, but at large bluntness, AOA effects reverse, and transition is windside forward and leeside aft. The initial nosetip surface roughness is reported as 16 microinches rms, but no after-run nosetip roughness was reported. Dan Reda (private communication, 2002) reports that NOL Tunnel 8, the facility used, was famous for blasting models with particles from the pebble-bed heater. Muir (private communication, 2002) stated that he believes they worried about repeating results, although no records of such repeated runs are available any more. Muir also stated that they never considered the effect of tunnel-induced roughness on the nosetip.

Martellucci et al. also measured transition on the windward and leeward rays of sharp and blunt cones at AOA, at Mach 8 [78]. A reversal of AOA effects from leeside-forward to windside-forward was also observed, as the nose bluntness increased from 1% to 2%.

Sakell measured transition on the windward and leeward rays of sharp and blunt 10-deg half-angle cones at AOA, at Mach 6 [79]. For the sharp cones, transition moved forward on the leeside ray and aft on the windward ray. As bluntness increased, transition moved aft at zero AOA. However, transition then became very sensitive to tunnel pressure, moving forward by 90% of the body length when stagnation pressure was increased by 10% (p. 9). For large bluntness, high unit Reynolds numbers were needed to obtain transition on the model, and AOA effects reversed to windside forward and leeside aft. For the 0.5-inch nose-radius cone, Fig. 65 shows transition reversing from leeside forward to windside forward as the tunnel stagnation pressure increased from 900 to 1400 psia. Clearly, there is a shift in mechanism, which Sakell was not able to explain. Sakell reports no measurements of nosetip roughness, and (private communication, 2002) did

not consider nosetip roughness generated by tunnel particulate.

Stetson measured transition on sharp and blunt cones at angle of attack in a Mach-6 tunnel [80]. On a sharp cone, the movement of transition with angle of attack depends on tunnel and Mach number (and noise levels [6]). However, transition always moves aft on the windward ray and forward on the leeward ray. On the windward ray of the blunt cone, transition first moves aft with AOA, and then forward with larger AOA. Transition always moves forward with AOA on the leeward ray. On the 2%-blunt-nosetip 8-deg half-angle cone, an AOA of 1 deg. moved transition forward by 50% on the leeward ray. Ref. [81] provides details on the sensitivity to nosetip roughness at large bluntness; due to tunnel-particulate sandblasting, the data becomes unrepeatable, at zero or nonzero AOA.

Holden measured transition on sharp and blunt cones at AOA at Mach 11 and 13 [82]. The data were reanalyzed in Ref. [83], and apparently combined with later data. For small-bluntness cones, transition moved forward on the leeward ray and aft on the windward ray. However, for the largest bluntness, this pattern reversed, and transition moved forward on both the windward and leeward rays (differing from Muir and Trujillo). Limited measurements also explore the marked effect of nosetip gouges on frustrum transition. Steps and gaps in the frustrum surface had a lesser effect on transition.

Thyson et al. put roughness trips and blowing trips just aft of the nose of a hypersonic blunt cone at AOA [84]. The trips cause transition to occur first on the windward side, since the boundary layer is thinner there. Thus, a shift from a smooth-wall stability-based mechanism to a roughness-induced one would tend to shift transition from leeside forward to windside forward.

For blunt and sharp 5-deg. half-angle cones at Mach 6, Bailey showed that transition can move center-of-pressure by about 4% for angles of attack of one or two degrees [85].

Johnson and Candler et al. computed the effect of chemistry on the stability of blunt cones at angle of attack [86]. Sharp and blunt cones are computed at 4 km/s and a 20 km altitude. Full nonequilibrium chemistry is included, but the linear stability analysis is presently limited to parallel flow without curvature terms. Bluntness stabilized the flow.

Summary

1. Both sharp and blunt cones are very sensitive to small AOA, especially for smaller nose radii.

2. Both sharp and blunt cones exhibit the cross-flow instability at angle of attack. Flow visualization shows clear evidence of these nearly-streamwise vortices, just like in low-speed measurements on swept wings. This suggests that the vortices can be induced under controlled conditions using very small roughness elements, as in Saric's work [12]. It also suggests that careful computations using the nonlinear parabolized stability equations could reproduce the experimentally measured amplification, and enable a physics-based prediction method.

3. For blunt cones at AOA, there is good evidence for a change from an apparently smooth-wall mechanism for small nose radii to a nosetip-roughness-related mechanism for larger nose radii. This change in mechanism would explain the reversal from leeward-forward transition at small nose radii to windward-forward transition at large radii. Careful measurements with small roughness on the nosetip should explain this phenomenom, which may be related to the transient-growth instability (e.g., Ref. [87]).

4. Experimental studies should be carried out in close coordination with computations. This should not be so difficult now, since codes for accurate computation of the mean-flow and linear instability are more accessible.

The Boeing/AFOSR Mach-6 Quiet Tunnel

Quiet facilities require low levels of noise in the inviscid flow entering the nozzle through the throat, and laminar boundary layers on the nozzle walls. These features make the noise level in quiet facilities an order of magnitude lower than in conventional facilities. To reach these low noise levels, conventional blow-down facilities must be extensively modified. Requirements include a 1 micron particle filter, a highly polished nozzle with bleed slots for the contraction-wall boundary layer, and a large settling chamber with screens and sintered-mesh plates for noise-reduction [5]. To reach these low noise levels in an affordable way, the Purdue facility has been

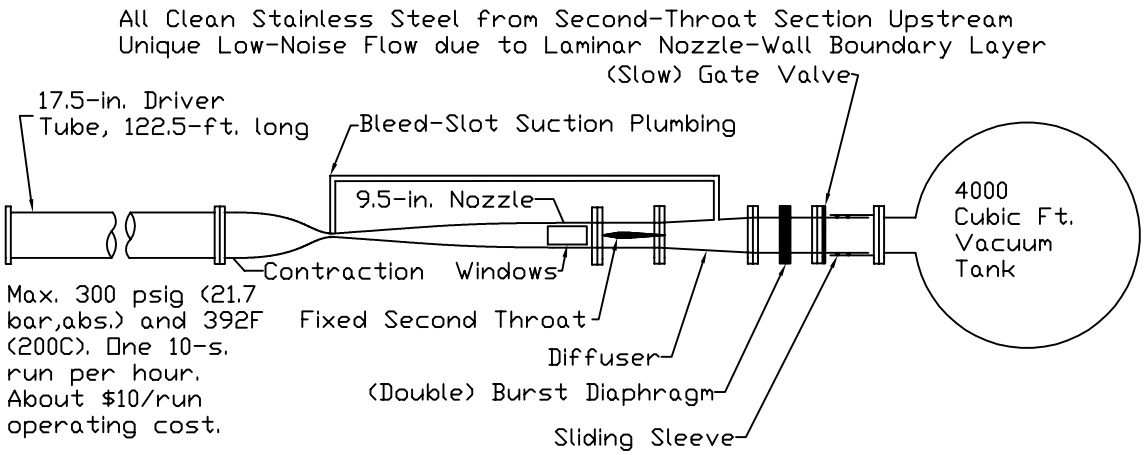

Figure 2: Schematic of Boeing/AFOSR Mach-6 Quiet Tunnel

designed as a Ludwieg tube [88]. A Ludwieg tube is a long pipe with a converging-diverging nozzle on the end, from which flow exits into the nozzle, test section, and second throat (Figure 2). A diaphragm is placed downstream of the test section. When the diaphragm bursts, an expansion wave travels upstream through the test section into the driver tube. Since the flow remains quiet after the wave reflects from the contraction, sufficient vacuum can extend the useful runtime to many cycles of expansion-wave reflection, during which the pressure drops quasi-statically.

Figure 3 shows the nozzle of the new facility. The region of useful quiet flow lies between the characteristics marking the onset of uniform flow, and the characteristics marking the upstream boundary of acoustic radiation from the onset of turbulence in the nozzle-wall boundary layer. The onset of turbulence is drawn for several computational predictions, although quiet flow has not yet been achieved at high Reynolds number. A 7.5-deg. sharp cone is also drawn on the figure. The cone is drawn at nearly the largest size for which it starts. More information about the facility can be found in Refs. [89] and [90].

Instrumentation Progress

Dewpoint Measurements

Dewpoint is important for understanding condensation effects. Measurements of dewpoint became possible after a Panametrics meter was installed in early summer 2002. It is connected just upstream of the double-diaphragm section, from where it can sample the air used to fill the driver tube and nozzle before the run begins. The sensor is an aluminim oxide element calibrated by the manufacturer, who quotes a range of $-90°C$ to $20°C$, with an accuracy of $3°C$ and a repeatability of $1°C$. Unfortunately, due to oversights, regular sampling has only recently begun, and few data are available from the humid summer period.

In early May, initial measurements were obtained of typical dewpoints while taking tunnel performance data for Case 6. In these runs, the dewpoint was always measured to be about $-20°C$.

Additional measurements were taken in December 2002. If the tunnel was emptied of air, and then refilled with dry air from the compressor, the dewpoint was about $-30°C$. The lower dewpoint is probably due to the low humidity of the winter air. In order to get an idea of a less desirable condition, the tunnel was emptied of air, then refilled to atmospheric pressure using ambient air. The tunnel was then filled to 45 psia with dry air, since the dewpoint can only be measured when there is positive pressure to allow air samples to pass through the dewpoint meter. This resulted in dewpoints ranging from $-10°C$ to $-15°C$. The dewpoint meter was also left on overnight with dry air constantly being bled into the tunnel and past the meter. By morning, the dewpoint was $-46°C$, which was therefore an approximation for the dewpoint of the air produced by the compressor and dryer on that day. However, worst-case dewpoints under hot and humid summer conditions have yet to be determined.

In all of the case 7 post-polish runs that were above atmospheric, the dewpoint was measured, and was always about $-30°C$. It is difficult to get much lower than this in an actual run since the tunnel

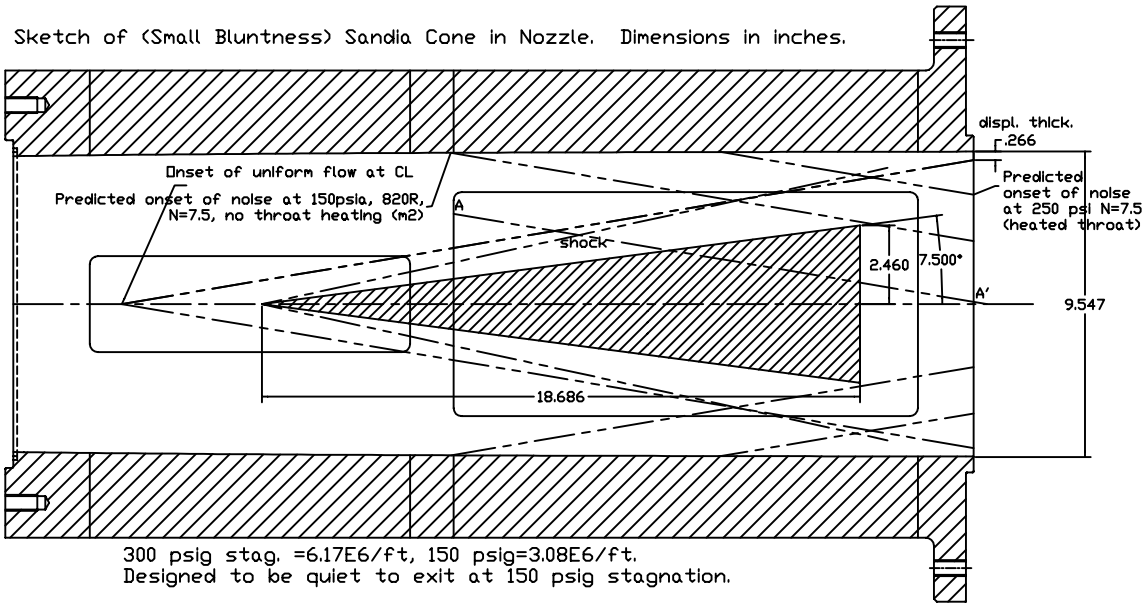

Figure 3: Schematic of Mach-6 Quiet Nozzle with Model

must be opened at least briefly to replace the diaphragms.

Automation of Burst Diaphragm Fabrication

Until recently, burst diaphragms were fabricated by hand in small batches using a jig in a CNC milling machine [91]. As this process was inefficient and awkward for continuing operations, a mass-production method was implemented. A die was designed and fabricated by AAA Tool and Die of South Bend, Indiana, in order to automatically stamp out the diaphragms from large rolls of sheet stock. The die was then used by the vendor to stamp out diaphragms from the remainder of three existing rolls of material; in addition two new rolls were procured and stamped out at the same time. The diaphragms were procured in large lots both to improve consistency and to reduce cost. Aluminum is used except for 1 atm. and below, where hand-cut acetate is used [92]. For the high and medium pressure runs, about 2750 of each of the 0.025-inch 5052-H32 and the 0.032-inch 3002-H14 diaphragms were stamped out. Only about 1000 of the low-pressure 0.008-inch 6061-O diaphragms were stamped, as those are not used as frequently. This provided a total of about 6500 diaphragms, enough for 3250 runs, which is several years supply at the current rate of usage.

New Digital Oscilloscope

A new Tektronix TDS7104 digital phosphor oscilloscope was purchased early in 2002. This 8-bit scope contains 4 channels, with 4MB of memory per channel, and has the option of combining channels to get 2 channels with 8MB each. Besides this improvement in memory over our past scopes (which stored 0.2-1 MB), the new scope features Hi-Res mode, where data is sampled at 1GHz and averaged on the fly into memory at the sampling rate. This provides additional resolution and digital filtering, both important for some of the data presented below.

Status of Quiet-Flow Performance

The tunnel remains quiet only at a very low stagnation pressure of about 8 psia, despite two major modifications that have been made since Ref. [89]. The modifications will be described, followed by the tunnel flow measurements, and an outline of future plans.

Design of Case 7 Throat Geometry

After initial quiet flow was achieved with the Case 6 throat geometry, a further attempt was made to improve the quiet flow Reynolds number through the Case 7 geometry. The Case 6 geometry is described in detail on pp. 10-12 of Ref. [89]. The Case 7 design followed a similar one-dimensional inviscid streamtube procedure, except that 1D flow was assumed on *both* the upper and lower sides of the bleed lip, for both the flow entering the suction slot and

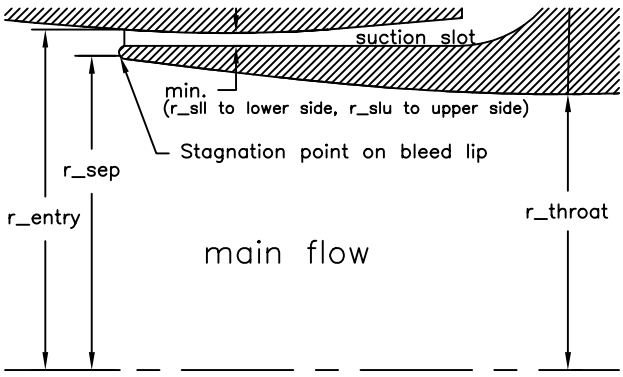

Figure 4: Detail Defining Critical Dimensions of Slot Throat

the flow entering the nozzle throat. This 1D assumption was made even in the neighborhood of the lip tip. This appears to be the procedure followed by Beckwith for the Langley nozzles [93].

Fig. 4 shows a generic detail of the slot itself, as revised from Ref. [89]. The radius of the upper wall at the bleed-lip tip is defined as '`r_entry`', the minimum height of the slot is defined as '`min`', with '`r_slu`' the radius to the upper side of the minimum and '`r_sll`' the radius to the lower side of the slot minimum. The radius to the separating-streamline stagnation point on the bleed-lip tip is '`r_sep`', and the radius of the main-flow throat is '`r_throat`'.

Since sonic flow from the same stagnation conditions is achieved at both the suction-slot throat and the main-flow throat, the area ratios from the slot entry must be the same:

$$\left(r_{entry}^2 - r_{sep}^2\right) / \left(r_{slu}^2 - r_{sll}^2\right) = r_{sep}^2 / r_{throat}^2. \quad (1)$$

Case 7 was designed using this full 1D analysis, and selecting the stagnation point to be 0.028 inches below the top of the 0.030-in. diam. bleed lip tip. The nominal suction fraction was increased to 38% from the 30% of Case 6. The increase in suction massflow makes the dia. of the bleed lip tip smaller relative to the slot size, and therefore makes it easier to put the stagnation point closer to the main-flow side of the tip. This should reduce the probability of a separation in the boundary layer on the main-flow side (although it increases the risk of a separation in the slot flow which might produce unsteady massflow there).

Table 3 from Ref. [89] is updated in Table 1. The symbol definitions are unchanged. The height ratio 'entry'/'min.' is taken as the area ratio A_{entry}/A^* in the annular slot. Using the area ratio in the slot, the pressure at the slot entrance, P_{se}, can be computed as a ratio to P_t, assuming sonic flow at the slot minimum. For the computations in the table, the slot entrance is taken to be the junction between the hemispherical tip and the upper surface of the bleed lip. This is again a 1D analysis in the slot. The width 'entry' is that at the slot entry, from the upper junction of the hemispherical tip, neglecting the tip diameter. The total pressure is P_t, $h_e(P_e/P_t = 0.82)$ is the theoretical slot entry height for which $P_{se}/P_t = 0.82$ and therefore matches the main-flow-side pressure, A_{entry} is the flow area in the slot at the entrance of the lip, and A^* is the sonic-flow area in the suction slot. Finally, $h_{e,tip}$ is the height from the top of the tip (which is 0.030-inch thick) at which the stagnation point of the separating streamline is nominally located.

For Cases 1-7 the analysis in Table 1 neglects the 0.030-in.-dia. bluntness of the bleed lip tip; although in designing Case 7 the 1D analysis is carried out right past the tip bluntness, the Case 7 listing in the table was carried out using the same method used for the other cases. This is why the value of 'hetip' (0.024 in.) differs from that implied by the location of the stagnation point that was used in the Case 7 design (0.028 in. from the top of the lip).

It was again noted that the Beckwith bleed-lip designs have a much larger angle with respect to contraction wall, so the angle was increased by an amount that was 1.6 degrees for Case 6 and 2.0 deg. for Case 7. This was as much as was possible with the present geometry while maintaining monotonic slopes in the contraction contour. Fig. 5 shows the modification to the geometry. The horizontal axis, z', is the axial contraction coordinate, where $z' = 0$ at the contraction entrance. The modifications were made to an insert that picks up the contour at $z' = 37.0$ in. The contour again makes a smooth joint at the match point, with a larger radius downstream, and with the difference in radius increasing monotonically.

Fig. 6 shows a drawing of the new geometry. The dimension is in inches. The upstream joint with the stainless-steel contraction section should be nearly flush. However, the contraction has not yet been disassembled from the upstream end so that the size of any discontinuity can be determined. It should be noted that both the Case 6 and Case 7 designs have the bleed lip moved upstream 0.250 inches compared to the earlier designs. This helped to make a larger angle with the contraction, and also enabled removing a Macor insulator disk. The insulator disk was a maintenance problem, and did little to insulate the throat section from the contraction.

Case:	1	2	3	4	5	6	7
entry, in.	0.036	0.036	0.036	0.073	0.073	0.1088	0.161
min. in.	0.029	0.029	0.036	0.042	0.062	0.1014	0.146
A_{entry}/A^*	1.24	1.24	1.0	1.74	1.18	1.073	1.10
P_{se}/P_t	0.81	0.81	0.53	0.91	0.78	0.70	0.73
$h_e(P_e/P_t = 0.82)$, in.	0.037	0.037	0.046	0.053	0.079	0.1288	0.185
$h_{e,tip}(0.82)$, in.	0.001	0.001	0.010	-0.020	0.006	0.020	0.024

Table 1: Properties of Bleed-Slot Geometries

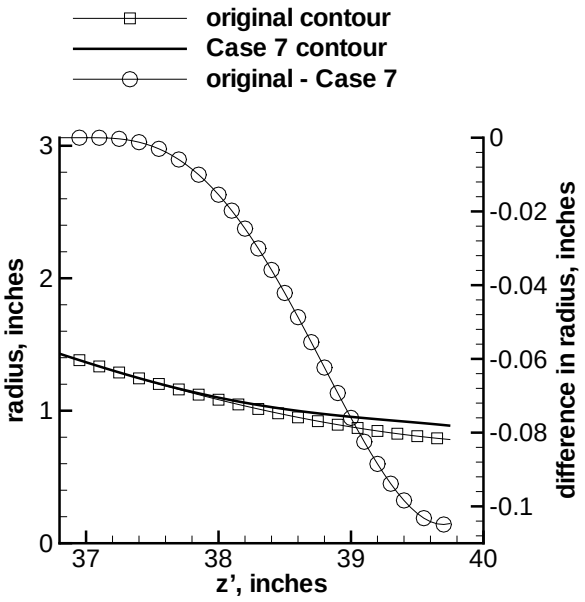

Figure 5: Modification to Contraction Contour, Case 7

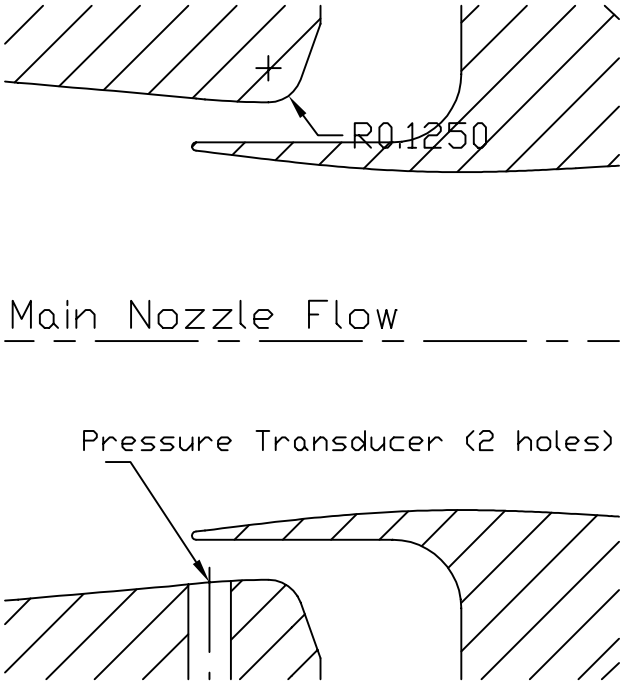

Figure 6: Drawing of Slot Throat, Case 7

Polish of Aft Portions of Nozzle

The electroformed throat region of the nozzle had earlier been polished to less than 1 microinch rms by Optical Technologies Inc. of Franklin Park, Illinois. This section ends at $z = 19.26$ inches downstream of the throat, where a small step was present between the electroform and the aft sections of the nozzle [94]. The downstream sections of the nozzle had not been polished, since the 16-32 microinch rms finish estimated from the lathe was much smaller than the 0.003-inch max. flaw height allowed even at $z = 19.26$ in. by the $Re_k = 12$ criteria (see pp. 4-6 of Ref. [94]).

Since the Langley Mach-6 nozzle was polished along the whole length, and was formed in a single 40-inch electroform without joints, the downstream portions of the present nozzle were polished in the hope that this would improve quiet-flow performance. Optical Technologies achieved an estimated 1-2 microinch rms finish over sections 4-7 of the nozzle, running from $z = 19.26$ to $z = 71.98$ inches, where z is the axial distance downstream of the nozzle throat. This finish was a little better in the upstream portion and a little less in the downstream portion. The polisher estimated that he removed 0.002-0.004 inches of material during the polishing, which should not change the contour significantly. The joints were all polished while assembled, so they should be smoother. In addition, the joint at the end of the electroform was smoothed as part of this polishing process. The polisher saw no degradation in the electroformed throat section and decided not to try to touch this section up.

The joints in the nozzle were checked by a Purdue machinist during assembly to get a rough idea of the stepsize that exists after polishing. Between sections 3 and 4, at the end of the electroform, the machininst estimated that the joint was better that 0.0001 inches all the way around. Between sections 4 and 5, there were a couple of locations with stepsizes getting up to about 0.0005 inches, but the joint was generally smoother than this. Between sections 5 and 6, the stepsize was better than 0.0002 inches. The largest stepsize is between sections 6 and 7, where it is generally about 0.0005 inches, but is up to 0.001 inches at one azimuthal location.

The polisher disassembled sections 5 and 6 of the nozzle as part of the polishing process. These sections had been received from the fabricator (DEI) as a unit, supposedly with an O-ring already installed, and had been operated for nearly 1-1/2 years. To our surprise, the polisher found no O-ring upon disassembly. Although soap-film bubble testing had not revealed any leaks at this joint, it seems likely that some leakage must still have existed despite the very tight precision lap joints that are used. High-temperature silicone o-rings were installed in the 4-5 joint upon reassembly; neoprene o-rings were used in the 6-7 and 7-8 joints, since these never rise substantially above room temperature.

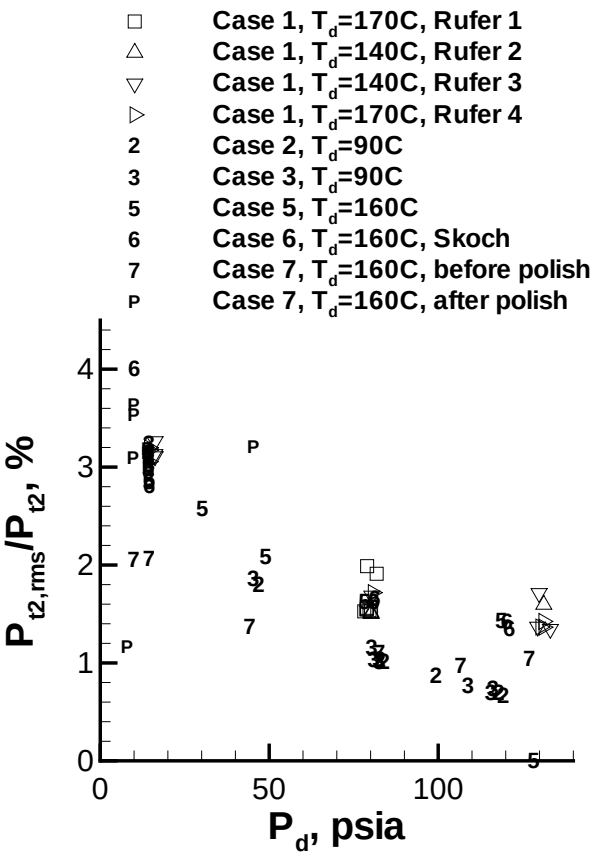

Figure 7: Pitot Fluctuations on Centerline

Pitot Measurements on Centerline Forward

Pitot measurements are made using a fast Kulite XCQ-062-15A pressure transducer, to determine the mean flow and fluctuations in the nozzle. Fig. 7 shows the pitot pressure fluctuations on the centerline ($\pm$ 1/16 in.), with the probe full forward on the traverse. The data for Cases 1, 6, and 7 (post-polish) were obtained at $z = 84.3 \pm 1/16$ in. The data for cases 2-4 and 7 (prepolish) were obtained at $z = 84.63 \pm 1/16$ in. The Case-5 data were obtained at $z = 84.16 \pm 1/16$ in. Cases 1-5 were reported in Ref. [90]. The data were sampled at 500kHz by 8-bit LeCroy digital oscilloscopes, except the Case 7 prepolish data, which were sampled at 100 kHz. The bleed-slot valves were open for all runs, which thus

had slot suction. The rms and mean values were obtained from the first 0.1 sec. after tunnel startup, between 0.25 and 0.35 s after the initial pressure drop. There is no major difference between the Case 6, Case 7 prepolish, and Case 7 postpolish runs, despite the changes in the bleed slot throat, the polish of the downstream sections of the nozzle, and the installation of the O-ring between sections 5 and 6. This was a disappointing surprise. In particular, it is remarkable that the quiet flow performance does not show significant improvement after the substantial polishing work on the downstream section of the nozzle.

The noise level for Case 7 is significantly lower at the lower pressures, which remains to be explained. The lower sampling rate seems unlikely to account for the difference, since the amount of power above 50kHz is usually small. The traces are not clipped on the analog electronics or the scope. The Case 7 postpolish data includes a point at about 1% fluctuations below $P_d = 10$ psia where the flow is intermittent.

Fig. 8 shows sample segments from pitot traces obtained at $z = 84.3$ inches on the centerline, all at an initial stagnation pressure of 10 psia and a stagnation temperature of $160°C$. The Case 6 data was acquired at 10kHz, the prepolish Case 7 data at 100kHz, and the postpolish Case 7 data at 200kHz. The complete traces for the three cases all show flow starting up at about 0.23-0.25 sec., followed by an initially noisy flow, which looks similar to part (a). The flow then appears to become intermittently quiet, with low noise regions in between small spikes, as in the period from 1.41 to 1.45 sec. in (b). This is followed by a period in which the small spikes are interspersed with larger spikes, as can be seen in (b) and (c). The full record clearly shows that Case 6 remains noisy longer, with quiet intervals being noticeable only at about 1.6 s, while they are noticeable in prepolish Case 7 at 0.6 s and in postpolish Case 7 at 0.3 s. Since the stagnation pressure drops about 5% every sec. after startup, this is a small but significant increase in quiet flow Reynolds number. Parts (a-c) of Fig. 8 show the 3 cases at an early time, where the difference between Cases 6 and 7 is evident.

The spikes clearly fall into two separate categories of large and small, for reasons yet unknown. The large spikes have an amplitude of about 0.1 psia. Since the mean pitot pressure at Mach 6 is about 3% of the stagnation pressure, and the stagnation pressure is about 8 psia at this time, the pitot pressure is roughly 0.2-0.3 psia, and the large spikes are of the order of 30-50% of the mean, which is very large. This suggests they are associated with intermittent separation of the nozzle-wall flow. However, they drop out later in the run when the pressure ratio decreases further, so they can hardly be associated with a simple unstart. It is curious that the end of the Case 7 postpolish run has 11 large spikes at a regular interval of about 5 ms right before the flow drops subsonic. The smaller spikes have an amplitude of 0.01-0.02 psi, which is roughly 5-10% of the mean, which seems reasonable for noise radiated from turbulent spots on the nozzle wall.

Parts (d-f) of Fig. 8 show a period later in the run. Case 6 in part (d) still has many spikes, both large and small, as it appears to drop quiet somewhat later. Parts (e) and (f) show that the pre- and post-polish Case 7 data now have a few large intermittent spikes in a primarily low-noise flow. The postpolish Case 7 data has a few more spikes in this segment, as is generally true for these records, so that the polishing made no clear improvement in quiet flow. Case 6 actually has only one large spike from 5.5-9.0 s, while Case 7 prepolish has 3 from 5.5 to 6.3 s before it drops subsonic early, and Case 7 postpolish has 3 spikes from 5.5 to 8.1 s before it starts to drop subsonic.

The quiet part of a run from a stagnation pressure of 8 psia and a stagnation temperature of $160°C$ was examined, to see what the residual noise level is when the spikes are absent. The probe was at $z = 84.3$ in. on the centerline, and the signal was sampled at 200kHz. The average stagnation pressure during the quiet interval was 6.7 psia, the average pitot pressure was 0.32 psia, and the uncorrected rms fluctuation level was 0.10%. The square root of the difference of squares was then taken to subtract the background electronic noise yielding a corrected rms noise level of 0.07%. The signal/noise ratio was 1.3 during the quiet portion. This background noise level is comparable to that achieved in the Mach-4 Ludwieg tube [88], and is more or less what is expected in a quiet tunnel.

Fig. 9(a) shows pitot fluctuations obtained at $z = 84.3$ in. on the centerline of the Mach-6 tunnel from a driver pressure of 10 psia and a driver temperature of 160C. The output of the XCQ-062-15A Kulite is amplified by a factor of 100, high-pass filtered at 800Hz, and then amplified by another factor of 100. This AC output is digitized using a new Tektronix TDS7104 8-bit scope at 200kHz in Hi-Res mode. In this mode, the scope runs the digitizers flat out at 1GHz full speed, averaging the data on the fly and placing the averages in memory every 5 microsec. This provides digital filtering of high-

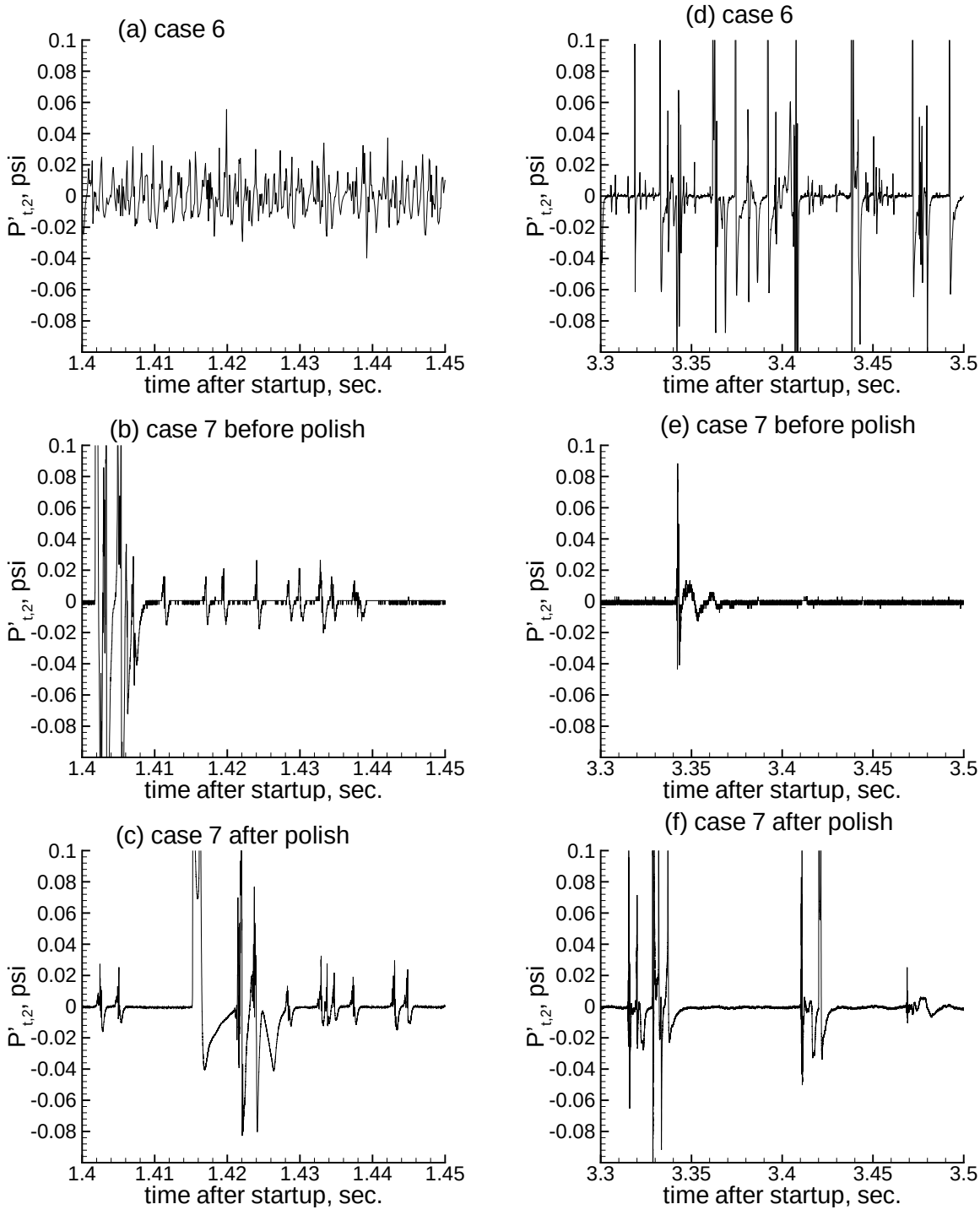

Figure 8: Samples from Traces for Three Cases

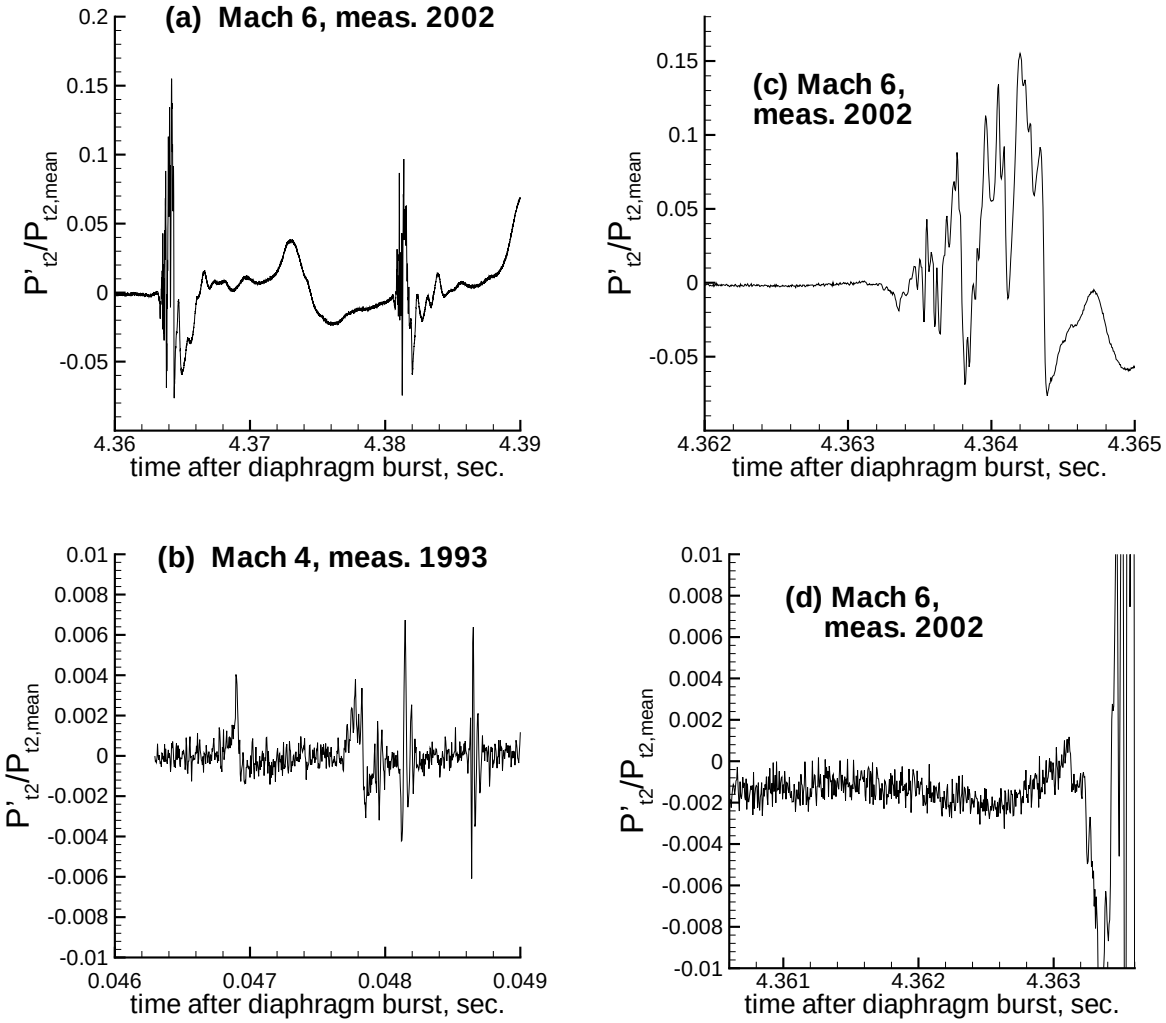

Figure 9: Sample Pitot Fluctuations at Mach 4 and 6

frequency noise, and also supplies, in this case, about 15 bits of resolution (as can be seen from detailed study of the digitized signal). The figure shows a quiet-flow interval from about 4.360 to 4.363 s., followed by a spike at about 4.364 s. The spikes are thought to be noise radiated from turbulent spots on the nozzle wall [88]. The peaks in the spikes are typically about 10-20% of the mean pitot pressure, which is about 0.47 psia.

Part (b) of Fig. 9 is replotted from Fig. 10 of Ref. [88], and was obtained in the Mach-4 quiet tunnel at 14.0 psia total pressure; the mean pitot pressure is about 1.9 psia. The spikes are again thought to be radiated noise from the passage of turbulent spots on the nozzle wall. Here, the peaks in the spikes are less than 1% of the mean pitot pressure, an order of magnitude smaller than in the Mach-6 tunnel. The cause of the much larger amplitude in the Mach 6 tunnel is not known, although Mach number effects are the obvious explanation.

Parts (c) and (d) are the same data shown in Part (a), but plotted on scales similar to those in Part (b). Part (c) shows a section of the Mach-6 data plotted over the same 3 ms period used in part (b). The spikes have a much longer duration than in the Mach-4 tunnel, possibly indicative of the irregular passage of turbulent spots that have a much larger physical extent. Part (d) shows a 3 ms interval plotted with a vertical scale similar to that used for the Mach-4 data. The peak-to-peak fluctuations in the low-noise portions are comparable in the two tunnels.

Fig. 10 shows the corresponding mean Mach numbers, from the same set of measurements. The Case 6 and Case 7 data is generally consistent with the earlier data, showing a mean Mach number of 5.7 to 6.0. There is one post-polish Case 7 datapoint at Mach 4.8 for $P_d < 10$ psia; this run is intermittently laminar. Here, Kendall suggests that separation is occuring on the nozzle walls for the laminar layer, reducing the mean Mach number.

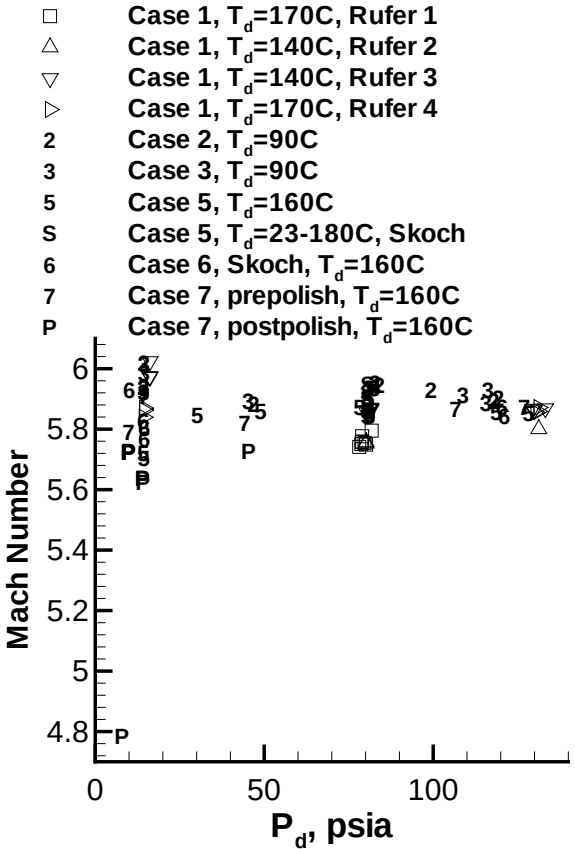

Figure 10: Mach Number on Centerline

Five runs were made at three initial driver pressures with the Case 7 postpolish configuration, again with the pitot sensor at $z = 84.3$ in. on the centerline, and at a driver temperature of $160°C$. The data were sampled with the Tek scope in Hi-Res mode at 200kHz. During the runs, the stagnation pressure drops, and the signal looks like Fig. 11. The flow starts up at about 0.2 s, there is about 1 s of moderate noise flow, then large spikes appear for about 1 s and the mean pitot signal rises by nearly a factor of 2. The spikes then gradually drop out as the stagnation pressure drops, until there is finally low-noise

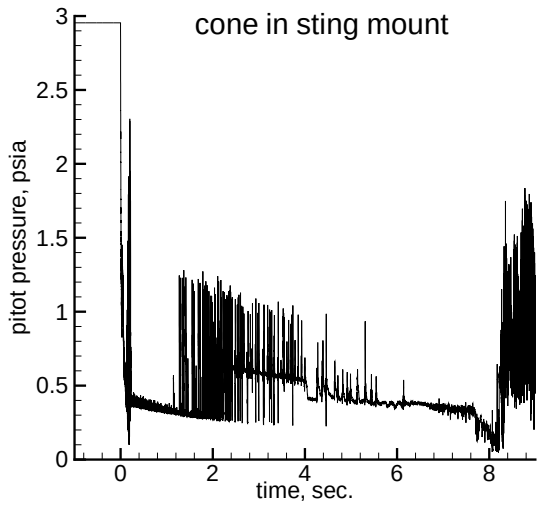

Figure 11: Pitot Fluctuations at 10 psia

flow.

The data from these five runs were averaged over 0.1-sec. intervals, which supplied the mean and rms pitot pressures and the mean stagnation pressure for each interval. The mean pressures were reduced to a local Mach number for the interval, and the data are plotted in Fig. 12. When the noise level is conventional above about 11 psia, the noise increases with decreasing pressure as the Mach number rises. The rising Mach number is the opposite to what one would expect, given thickening boundary layers, and must be related to the movement of transition on the nozzle walls. From about 10.5 to 9.5 psia, the noise starts to fall as the Mach number remains nearly constant. From about 9.5 to 8 psia, the noise jumps up as the intermittent spikes appear in the traces. The mean Mach number falls rapidly as the mean pitot pressure rises. Below about 8 psia, the noise level is low, the Mach number starts low and rises as the pressure drops further. As Kendall has suggested, this seems to be good evidence for separation occuring on the nozzle walls as the wall layers drop laminar. The separation reduces the flow area and the Mach number. The separation is apparently associated with a low noise level. It remains to be understood how the flow can separate in a diverging but nearly straight nozzle. It appears to be related to the upstream influence of shock-boundary-layer interactions in the diffuser. If this diffuser can affect separation, it seems likely that it might also be affecting transition.

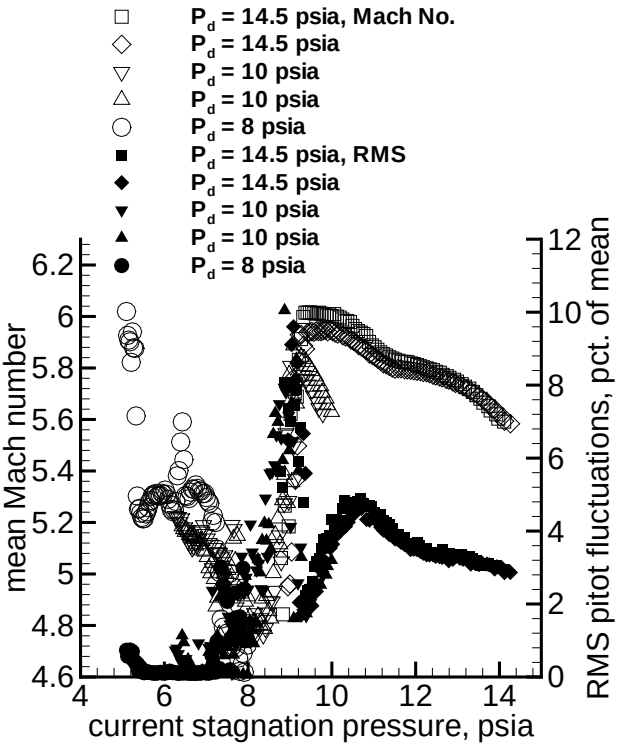

Figure 12: Runtime Variations of Mach Number and Pitot Fluctuations

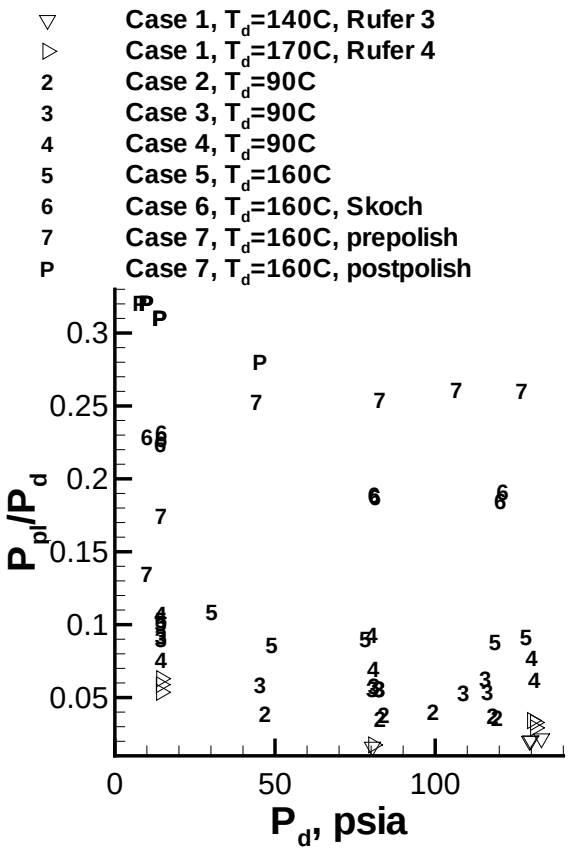

Figure 13: Mean Pressure in Suction Plenum for Bleed Slot

No data exists for the mean pressure in the bleed-slot throat for Case 7, due to the failure of the transducer. The data for Case 6 has not yet been reduced.

Fig. 13 shows the mean pressure in the plenum for the bleed-slot suction, normalized by the upstream driver pressure. The values are all well below 0.528, suggesting that sonic flow is successfully achieved in the slot, preventing the upstream transmission of noise from the bleed plumbing. The pressure rises with the massflow through the slot. The data for Case 7 before the polish show a marked drop at low pressures that remains unexplained.

Data from the contraction wall transducer is not shown here. The mean pressure is used to determine the time dependence of the driver tube pressure, since the diameter at the transducer is 17.412 in., very near the 17.500 in. at the contraction entrance. The rms fluctuations on this sensor have in all cases been equal before and after the run started, so any static pressure fluctuations in the driver tube have a signal/noise ratio of 1, and are less than 0.1% in amplitude [90].

Pitot Profile Measurements in Nozzle

The newly automated probe traversing system (Ref. [89]) has been used to measure mean flow profiles far forward in the test section of the BAM6QT. The new developments to the traverse allowed the probe to be moved during the run, expediting the data acquisition process. Previous data were taken with the probe stationary. A new, 12-in long pitot probe allowed profile measurements to be made far forward in the test section for the first time [95].

Mean flow profile data were taken at three initial driver tube pressures, 14.4, 75, and 135 psia, at stagnation temperatures of around 780 deg. R (initial freestream Reynolds numbers of 3.7×10^5/ft., 1.8×10^6/ft., and 3.2×10^6/ft., respectively). The freestream Reynolds number drops 30, 19, and 19% while the probe is moving during the three runs; the larger percentage drop at the lower pressure remains to be explained. Prior to the series of runs, the Test Section Reference Jig was used to position the probe at the nozzle centerline, 76.0 ± 0.2 inches downstream of the throat. The motion-control program triggered from the initial pitot pressure drop at the start of the tunnel run. The probe remained at its initial position for 0.32 s; 0.22 s to wait for the start-up noise to drop out and 0.1 s for the first data period. The probe then moved up one inch in 0.758 s to the second profile station, where it waited 0.1 s to take data. It repeated this movement three more times, waiting 0.2 s after the final movement at the top of the stroke. The probe then moved down through four one-inch steps, taking data for 0.1 s at each station. Thus, the probe captured two sets of data at each of five stations across the test section in one run. The stagnation pressure was recorded continuously throughout the run using the Kulite pressure transducer at the contraction entrance.

Four sets of data were taken for each initial driver pressure, two with the probe starting at the tunnel centerline and two with the probe starting 0.5 inches below this. This resulted in mean flow profiles consisting of ten points spanning 4.5 inches across the test section. The top station was about 0.7 inches from the wall.

The average Mach number at each profile station was determined using the isentropic formula relating pitot and stagnation pressure (eqn. 6.1 in Ref. [96]). The Reynolds number in the tunnel at each profile station was determined from the stagnation pressure and temperature (in the driver tube) and

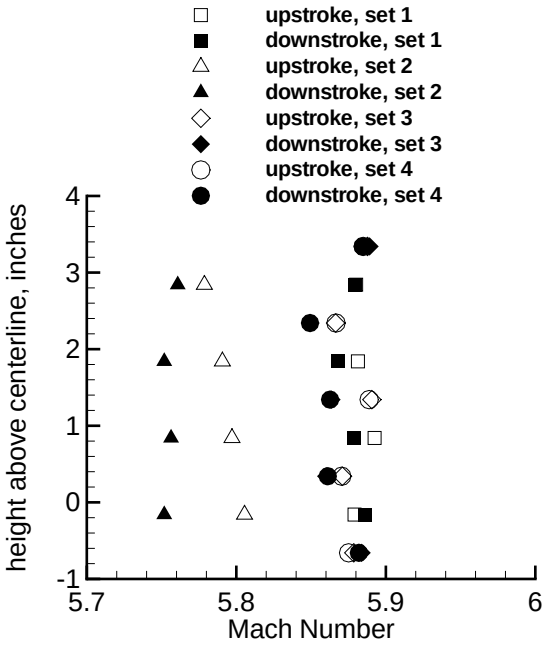

Figure 14: Mach Number Profiles at 135 psia

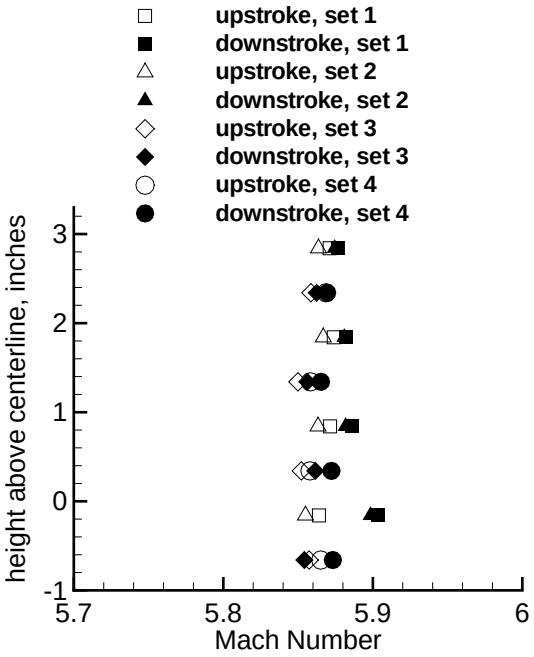

Figure 15: Mach Number Profiles at 75 psia

the Mach number at the profile station. Stagnation temperature was found from the isentropic relations described in Ref. [97]. The predicted stagnation pressure was a few percent lower than the measurement.

The Mach number profile for the 135-psia data is shown in Fig. 14. Three of the four runs show a fairly uniform core flow with a mean Mach number of 5.88. The other set with a lower Mach number was the first run of the day, and probably shows the effect of poorly controlled humidity. The tunnel-air dewpoint for this data is unknown. Points taken in the nozzle-wall boundary layer are here omitted.

The Mach number profile for 75 psia is seen in Figure 15. All four data sets show a uniform core flow around M = 5.87. The points within the (thicker) boundary layer are again omitted. The increase in Mach number near the centerline during the run may indicate that a wave becomes focused there as the Mach angle and boundary layer state change during the run. This wave may be caused by an axisymmetric step in the tunnel contour.

Figure 16 shows the Mach number profile for a driver pressure of 14.4 psia. The mean Mach number in the core flow is 6.00. The Mach number increases throughout the run. This is opposite to the effect expected with a thickening boundary layer. This increase may be due to movement of

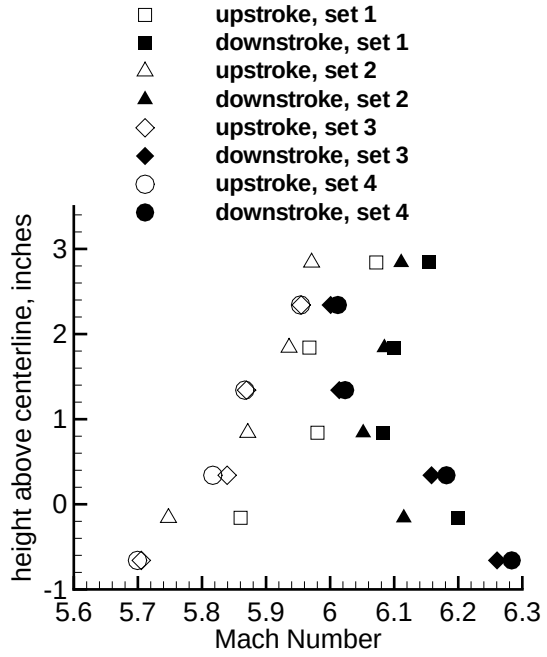

Figure 16: Mach Number Profiles at 14.4 psia

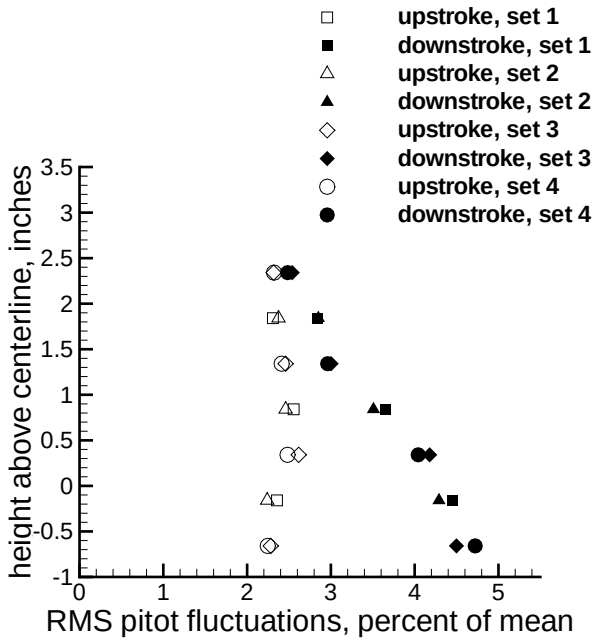

Figure 17: Pitot-Fluctuation Profiles at 14.4 psia

transition in the nozzle-wall boundary layer as the run progresses.

The RMS noise profile is shown in Fig. 17. The noise increases throughout the run; points within the nozzle-wall boundary layer are again omitted here. The measurements are generally consistent with earlier measurements; the tunnel is still not running quiet. Noise data are not included for the 75- and 135-psia data due to problems with the data acquisition settings.

The accuracy of the traverse system will be determined by viewing the motion of the probe with a telescope and measuring the distance between the probe and the Reference Jig after a movement. More accurate flow profiles will be acquired with more data points across the test section. The methods used to acquire this data will be used to investigate the boundary layer on a cone and the Hyper2000 model.

Effect of Downstream Perturbations on Upstream Noise

When the tunnel began operation in April 2001, effects of the diffuser configuration on the upstream pitot measurements were immediately noted. Fig. 18 shows a typical result. These pitot-fluctuation records were also obtained with the Kulite mounted on the centerline at $z = 84.3$ inches, using the Tek scope in Hi-Res mode at 200kHz. The initial driver tube pressure was 80.0 psia for both runs, and the initial driver temperature was $160°C$. The lower plot shows the results when nothing is mounted in the sting support boss on the front of the centerbody forming the second throat. The pitot fluctuations are very large, about 25% of the mean, although the mean pitot pressure suggests a Mach number of about 5.5, which is not far from the expected result. This sting-support boss is at $z = 104.990$ in., some 20.7 inches downstream. It is 2 inches in diameter, on the center of a plate with wedge leading and trailing edges that spans the cylindrical double-wedge section (Fig. 9 in Ref. [98]). The center of the boss has a cylindrical opening (for wire passage) which connects to openings in the side of the centerbody. Thus, ram-air jets out of the sides of the centerbody when nothing is mounted in the sting-support boss. It was thought that this ram air interferes with the tunnel startup process.

A small 2-in. diam. cone was therefore mounted in the sting support for all empty-tunnel runs (except those discussed in this subsection). The cone has a small nose radius of perhaps 1/8-1/4 inch, and a half angle of perhaps 30 deg. When this cone is mounted in the sting support, again about 20 inches aft, the upper trace from Fig. 18 results. The pitot fluctuations are now about 3% of the mean, with a mean Mach number of 5.8; these are the conventional values normally reported. At an initial driver pressure of 80 psia, there is thus a large effect on the upstream flow of the diffuser configuration well downstream. The shocks from the centerbody must impinge on the wall, with the pressure rise and pressure fluctuations being fed upstream through the subsonic part of the wall boundary layer, causing oscillations to be radiated onto the centerline pitot probe.

This behavior has been studied more closely recently. If data like that in Fig. 18 is generated at 45 psia driver pressure, the results are very similar. However, if Fig. 18 is generated at 130 psia driver pressure, the results are very different, in that both the empty-sting-mount and the cone-mount cases both show 'normal' flow, similar to the upper part of Fig. 18.

The results at a driver pressure of 14 psia are more curious, as shown in Fig. 19. The upper part (at $P_d = 14.34$ psia) shows normal flow, with the small cone mounted in the sting support. Spikes appear near the end of the run, as in the earlier plots. The middle portion (at $P_d = 14.57$ psia) shows the empty-mount case, which has high fluctuations but

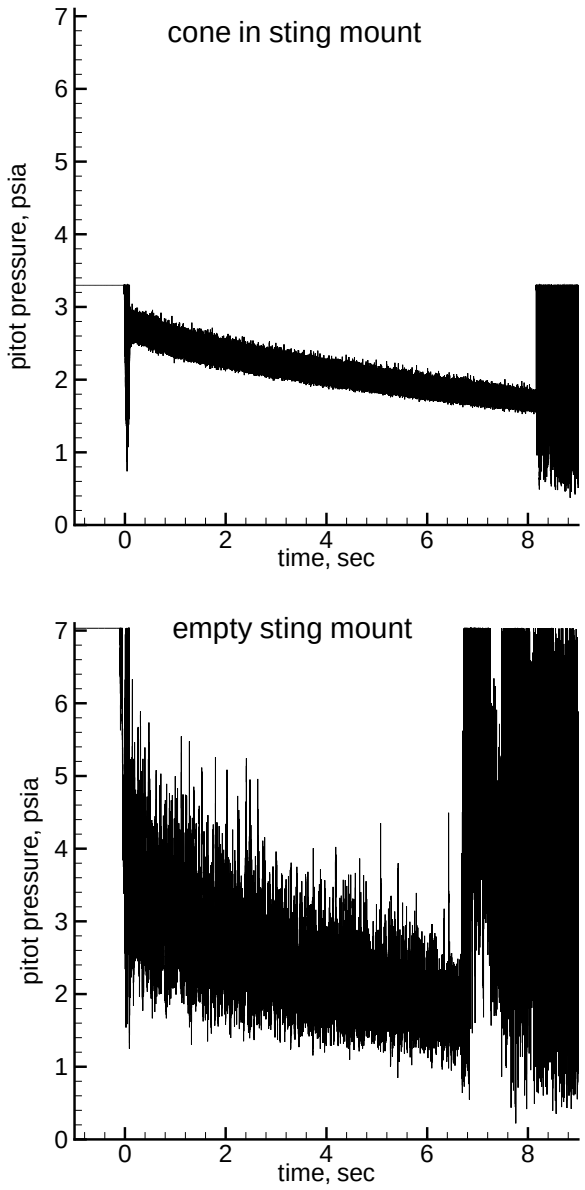

Figure 18: Pitot Fluctuations at 80 psia with Different Aft Configurations

low mean for the first 4 s, followed by 1 s of very high fluctuations, 1 s of low fluctuations and low mean, and 1 s of spikes in a low mean. The bottom portion shows the results when a 2-inch-dia. flat-faced cylinder is mounted in the sting support. The results are similar to the middle portion, except that the fluctuations in the first part of the run are much higher.

The results at 10 and 8 psia driver pressure all look like Fig. 11, no matter whether the cone, cylinder, or nothing is mounted in the sting support boss. Furthermore, these traces are repeatable, as is evident even in Fig. 12.

These results show that very substantial upstream effects are caused by the diffuser flow well downstream. These effects are currently the major focus of our work. Kendall suggests that the large rises in pitot pressure are due to separation of the nozzle-wall flow, or even upstream shocks. If the downstream conditions can cause these large upstream effects, could they not also be tripping the upstream flow to turbulence?

Quiet Flow Issues: What Next?

The primary tunnel issue remains the achievement of quiet flow at high Reynolds number. It is clear that a number of important issues regarding the tunnel operation remain to be resolved.

Possible causes of the early transition on the nozzle wall include [89]:

1. Fluctuations generated at the nozzle throat due to problems with the bleed-slot flow. This is thought unlikely, since the Case 6 and 7 slot-throat designs provide similar performance. However, it remains possible.

2. Fluctuations at the nozzle throat due to vibrations of the bleed lip. This seems unlikely, since the high frequencies likely to be effective are not transmitted well in the structure. However, it remains to be ruled out. The Mach-4 Ludwieg tube at Purdue ran quiet at low Reynolds numbers with similar vibration levels, but did not have a bleed lip, which might possibly enhance vibrational effects.

3. The rearward-facing step at the downstream end of the electroform [94]. This has been a concern; however, the recent polishing of the downstream part of the nozzle substantially reduced this step, but had no effect.

4. Insufficient polish on the downstream nozzle sections. This was a concern, since the downstream sections of the Langley Mach-6 nozzle

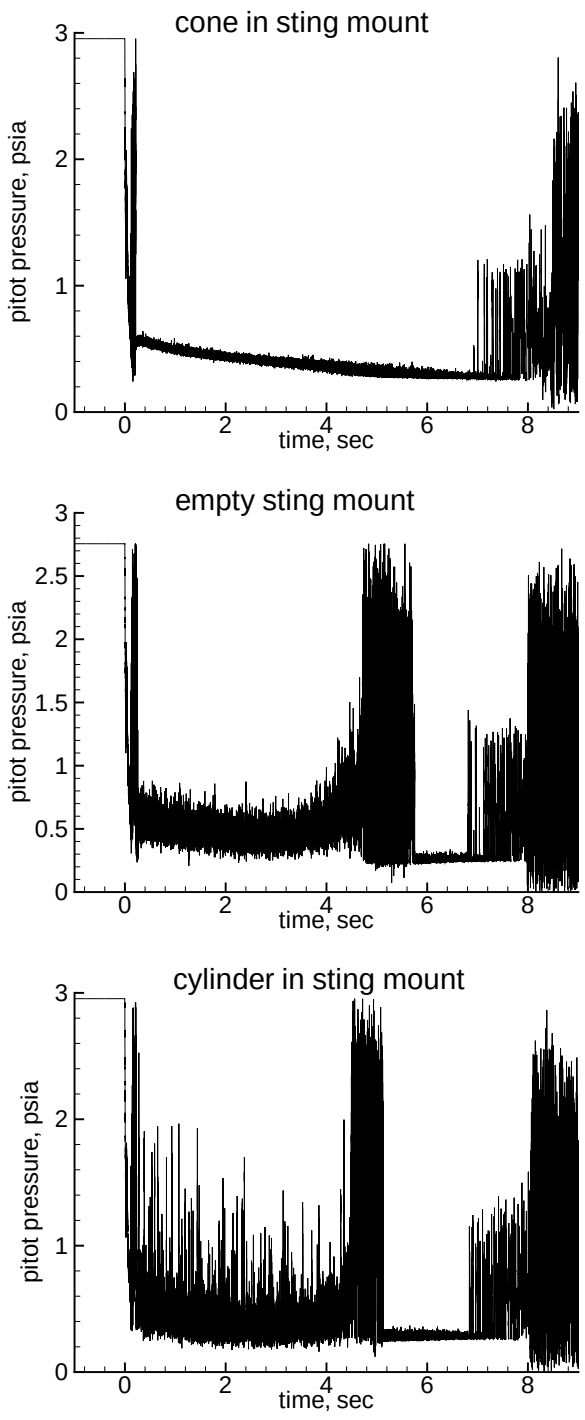

Figure 19: Pitot Fluctuations at 14 psia with Different Aft Configurations

were apparently polished beyond the $Re_k = 12$ criterion shown in Fig. 15 of Ref. [99]. However, the recent polishing of the downstream portion of the nozzle was a considerable improvement on the earlier finish and had no discernable effect.

5. Leaks in the nozzle or driver tube which cause disturbances. The existing joints have been checked for bubbling with a soap film solution; however, this failed to detect any leaks that occurred between sections 5 and 6 due to the lack of an O-ring. Kendall has stated (private communications, 1995-2002) that small leaks in the settling chamber of the JPL tunnel precluded quiet flow operation. A typical cause he reports is a loose bolt or other sealing flaw. It may be that small leaks remain in our system, and that these are tripping the flow. A more thorough leak check is in order.

6. The effect of diffuser conditions on the upstream flow.

7. Some other problem, such as noise in the driver tube that doesn't show up in the low-noise pressure measurements made on the contraction wall.

8. A nozzle-wall temperature distribution that decreases much more rapidly downstream than was initially expected. Although this might cause a reduction in quiet flow, linear-instability computations with a good approximation to the as-built temperature distribution suggested this would have only a small effect [91].

9. Some fundamental problem with the use of a very long nozzle which is not captured by the e^N analysis. This remains possible. However, it is hard to see how lengthening the nozzle by a factor of 2 compared to the Langley design could reduce the quiet flow pressure by more than an order of magnitude.

The following issues are to be addressed soon as part of the effort to obtain quiet flow:

1. An electrically controlled shut-off valve has been plumbed in the pipe that supplies air to the upstream end of the driver tube. This will enable blocking any air that might jet into the driver tube from the circulation heater during the run.

2. More leak checks are to be performed, using a helium sniffer borrowed from NASA Langley. Also, leak rates will be determined.

3. The effects of noise transmitted upstream from the diffuser will be investigated, along with the general operation of the diffuser system.

4. Hot-wire measurements are to be performed in the contraction entrance to ensure that the flow entering the throat is low noise.

5. Oil-flow measurements are to be made on the nozzle walls to look for signs of the Görtler instability (as in Ref. [100]).

6. The boundary layers along the middle of the nozzle wall are to be probed using a sled support that rides on the wall.

Temperature-Paints Measurements on the Hyper2000

Temperature Sensitive Paints technique (TSP) is being used to measure streamwise stationary instabilities on a generic scramjet forebody, whose geometry is very similar to the Hyper-X. Early results from a proof-of-concept experiment are shown in Ref. [89]. Since then, progress has been made in improving the instrumentation and measurement technique, several more experiments have been carried out on different roughness configurations that generate the disturbances, and in the development of data analysis techniques. The details of the measurement technique and the experimental results will be presented in detail in future papers [101, 102, 103], and only a summary will be given here.

Figure 20 is an image from a recent set of data. The total pressure and temperature was 120 psia and 763 deg. R respectively, giving a unit Reynolds number of 2,613,000/ft. The temperature of the model and TSP layer prior to tunnel run was 545 deg. R. A total of 17 roughness strips with a thickness of 0.00175 inches thick (7 layers) were used. The strips were spaced 0.15 to 0.16 inches on centerline, with each strip being 0.02 to 0.03 inches wide. Streak patterns can be seen, which are caused by the vortices generated by the roughness strips and their enhanced heating. The compression corners are located at 7.24 and 9.84 inches from the leading edge.

The variations in the heat transfer rate along the span at several streamwise locations are shown in Figure 21. Upstream of the first corner at 6.9 inches, the fluctuations are very small; no preferred wavelength seems to arise above the noise. Then the fluctuations grow, up to 9.1 inches from the leading edge. These fluctuations correspond to the streak structures shown in Figure 20. Beginning at about 10.4 inches, the amplitude of the fluctuations decrease, but the mean heat transfer rate increases. This might be the onset of turbulent flow, although hot-wire measurements are not yet available to confirm this hypothesis.

Figure 22 shows the power spectral densities for the spanwise heating distributions shown in Figure 21. The spectrum at the upstream most location is nearly flat, with no significant peaks relative to the other three data sets. A fluctuation at about 6 cycles/inch then grows from 7.8 inches to 9.1 inches, which corresponds to the streaks seen in Figures 20 and 21. The power of that wavenumber then decreases at 10.4 inches, which again would be caused if the boundary layers transitioned to turbulent flow. The spectral analysis method is currently being refined for more accuracy, and also to filter out low frequency noise, such as the peak seen around 1 and 3 cycles/inch.

The growth rates of the streaks are currently quantified by normalizing the power levels of each wavenumber along the model downstream coordinate by an initial power level. The initial power level is computed by averaging the power of the corresponding wavenumbers up to the first compression corner, in an attempt to average out as much of the noise as possible. The results for the data in Figure 20 are shown in Figure 23. The dominant wavenumber lays around 5.81-6.71 cycles/inch, which grow rapidly by a factor of about 300-350 past the first compression corner and then decay.

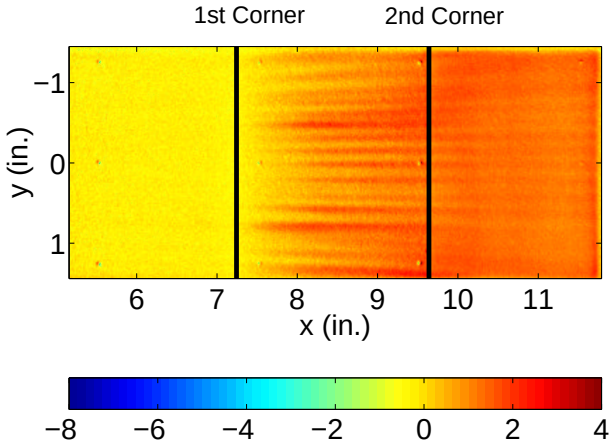

Figure 20: Heat Transfer Rate on Hyper2000 (W/cm^2)

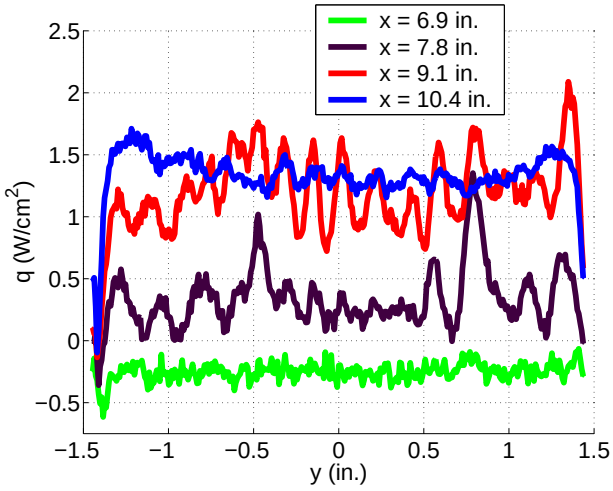

Figure 21: Spanwise Heat Transfer Rate Distributions on Hyper2000

Although this technique seems promising, the problem becomes apparent when a parametric trend such as that due to unit Reynolds numbers is examined, shown in Figure 24. For all tunnel runs here, 17 roughness tapes 0.002 in. thick were used, and the total temperature was 756 ± 18 deg. R. The unit Reynolds number was varied, by changing the total pressure from 1 atm up to 120 psia. The maximum growth rates for three wavenumbers are shown against the unit Reynolds number. It would be expected that the maximum growth rate should increase monotonically with the unit Reynolds number. The maximum growth rate for the 6.71 cycles/inch wave appears to follow that trend, however the remaining two plots seem to fluctuate sig-

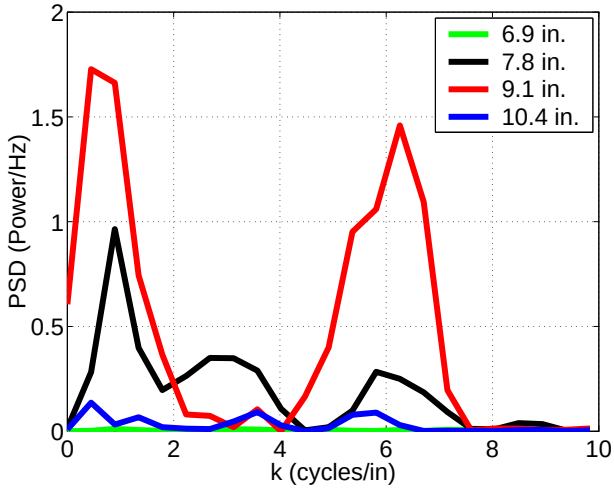

Figure 22: Power Spectral Densities of the Spanwise Heat Transfer Rate Distributions

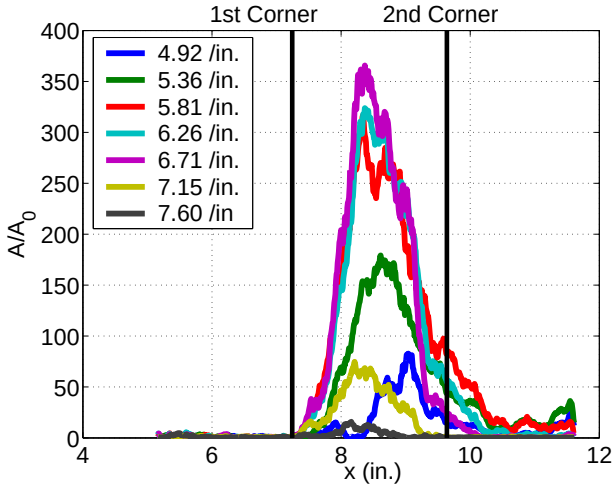

Figure 23: Integrated Growth Rates of Several Wavenumbers Along the Model

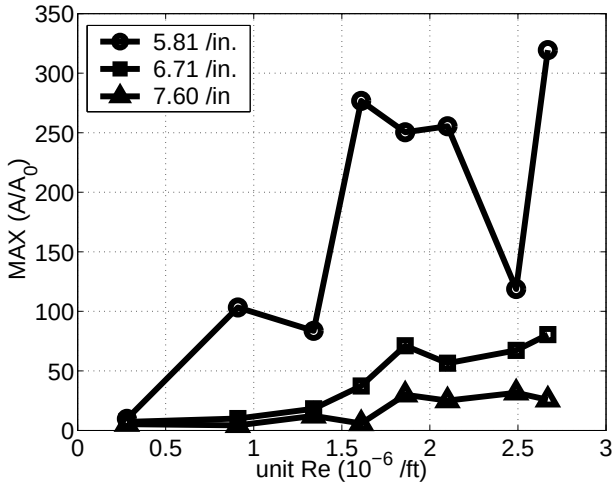

Figure 24: Unit Reynolds Number Effect on the Maximum Growth Rates for Several Wavenumbers

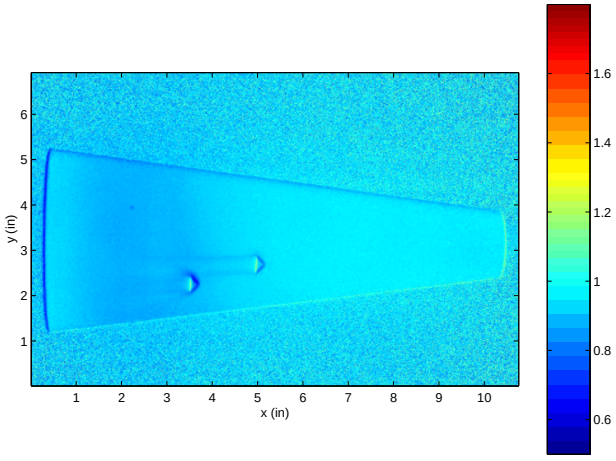

Figure 25: Sharp Cone at 0-deg. Angle of Attack

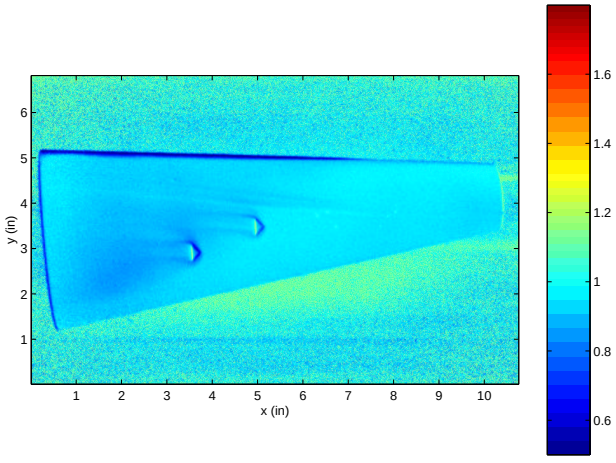

Figure 26: Sharp Cone at 6-deg. Angle of Attack

nificantly. The problem is probably because the initial wave amplitudes are not being computed with enough accuracy with the current method. Work is being done to address and correct this problem for future sets of experiments.

Temperature-Paint Measurements on Cones

In addition, two 7-deg. half-angle cones were fabricated with 4.0-inch and 5.5-inch base diameters, and with replaceable nosetips. Besides a sharp nosetip, the radii were 0.25 and 0.50 inches. These models are being studied with temperature-sensitive paint at zero, 3, and 6-deg. AOA.

The temperature sensitive paint technique was used to visualize boundary layer transition and streamwise vortices on a sharp, 7-deg. half-angle cone at 0 and 6-deg. angles of attack. Streamwise vortices, including crossflow vortices on a pitched cone, may play a role in the transition of the boundary layer to a turbulent state. A qualitative exploration of the parameter space was made to determine under which conditions (Re and AoA) streamwise vortices could be observed. Results with blunt cones have so far been inconclusive.

Two cone frusta were produced: one with a base radius of 2 inches and another with a base radius of 2.75 inches. The 2-in frustum was used for these experiments. The larger frustum will provide higher Reynolds numbers for future experiments. Three nosetips were produced: a sharp nosetip (nose radius of 0.002 in); and two blunt nosetips with radii of 0.25 and 0.5 in. The nosetips screw into the front of the cone frustum. The cone frusta screw into 2-in diameter high-strength steel stings. Two of the stings have slanted faces that allow the cone to be pitched to 3-deg. or 6-deg. angle of attack. The stings are designed so that the cone frustum is visible through the Plexiglas window in the side of the tunnel. Two triangular roughness elements were glued to the 2-in frustum after painting and before the experiments began. These roughnesses were made of 0.030-in thick shim stock and remained on the cone throughout the experiment. Later, microroughness elements were applied to the nosetip, and roughness elements of thinner shim stock were applied to the lower-front portion of the cone frustum. Temperature-sensitive paints were again used for the measurements [95]. The stagnation temperatures were held at about 780 Rankine ($160°C$) while the cones began the runs near room temperature.

The transition region on the cone at zero angle of attack was observed as a dark blue band around the back of the cone, as shown in Fig. 25 at a freestream Reynolds number of 3.04×10^6/ft. The intensity ratio is lower here than over the rest of the cone, since the heat transfer to the cone surface is higher underneath the transitioning boundary layer. Trailing vortices caused by the top triangular roughness element were also observed on the cone. The vortices are indicated by the blue streaks extending back from the tips of the triangle. The vortices cause high convective heat transfer to the cone, resulting in a lower intensity of emission from the paint underneath them. Leeside forward transition was observed on the cone at 6-deg. angle of attack, as shown in Figure 26 at a freestream Reynolds number of 3.06×10^6/ft. The trailing vortices from the 0.030-in roughnesses were also observed for this configuration. Two streaks above the trailing vortices appear to be crossflow vortices. These vortices do not come from a large roughness on the surface of the cone and are in the streamwise direction, as indicated by the trailing vortices below them. Later images showed that no crossflow vortices were seen as the result of microroughness or shims of less than 0.010-in thickness. The 0.010-in shim did produce a weak trailing vortex.

The vortices are washed out in the turbulent region. This causes a problem in observing the vortices. As Reynolds number drops, the transition region moves to the rear of the cone, but the boundary layer thickens and the roughness elements are less effective, resulting in weaker vortices. A more sensitive paint and a higher quality paint layer would help resolve the weaker vortices.

Future plans include the use of a more sensitive TSP in an attempt to visualize crossflow vortices on pitched sharp- and blunt-nosed cones. Microroughness dots will be placed on the nosetip and frustum in an attempt to stimulate the vortices. New blunt nosetips will be fabricated and sandblasted to create distributed-roughness. Attempts to visualize streamwise vortices and transition on the blunt cones at zero angle of attack will continue. Microroughness dots will be placed on the nosetip to simulate roughness caused by ablation of the heat shield on the nose of an RV. An automatic camera triggering system will be developed.

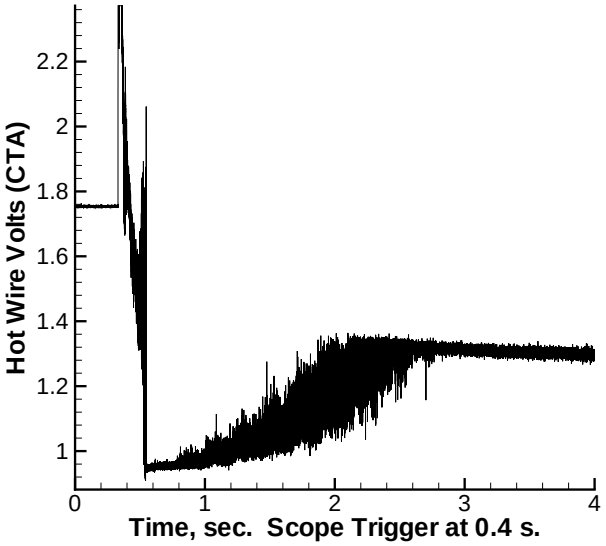

Figure 27: Single-Run Hot-Wire Profile of Sharp-Cone Boundary Layer

Preliminary Hot-Wire Measurements on a Sharp Cone

The automated vertical traverse is now operational, although refinements are still needed. Fig. 27 shows an uncalibrated preliminary hot-wire signal obtained during a single tunnel run. These measurements were made on a 7-deg. half-angle sharp cone having a 4.5-inch base diameter, at zero angle of attack. The wire is positioned 11.15 inches downstream from the tip of the cone. The total pressure was about 45 psia and the total temperature about 417K. The Reynolds number based on freestream conditions and the arc-length to the wire is about 1 million. A Pt/10%Rh wire is used, with a diameter of 0.00015 inch and a length/diameter ratio of about 160. A TSI IFA-100 constant-temperature anemometer is used, at an overheat of 1.8, so the output is primarily sensitive to mass-flow fluctuations. The square-wave frequency response measured in still air before the run is about 250 kHz. The data in Fig. 27 was sampled at 500kHz for 4 sec. using a Tektronix 7104 digital scope.

The first 0.3 s. in Fig. 27 is pretrigger data from before the start of the run, showing quiescent conditions. The scope triggers at 0.4 s, during the 0.25 s tunnel startup. The wire is initially positioned about 0.4 mm above the wall. At $t = 0.72$ s in the figure, the traverse begins to move the wire vertically away from the horizontal cone. The wire is

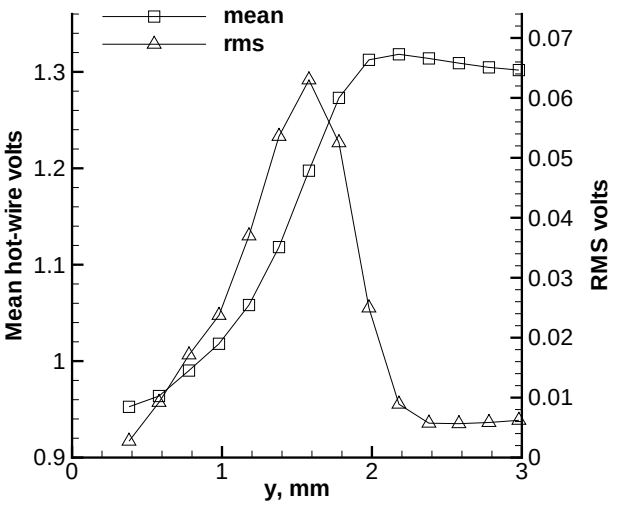

Figure 28: Boundary-Layer Profile from Single Tunnel Run

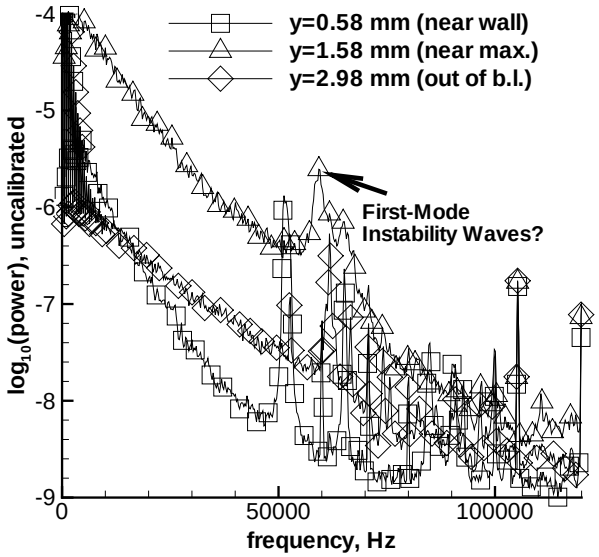

Figure 29: Hot-Wire Spectra from Sharp-Cone Boundary Layer

moved 0.2 mm in 0.127 s, remains stationary for 0.1 s, and repeats the process for 20 steps, ending up 4.4 mm above the wall. The trace shows the low mean massflux and low fluctuation levels expected near the wall. As the wire rises, the mean massflux rises, as do the fluctuation levels, which both peak near the boundary-layer edge. As the wire exits the boundary layer, the fluctuation levels decrease to the near-constant freestream level. The mean massflux outside the boundary layer should show a slight decrease due to the inviscid conical flow, but the mean voltage drop in Fig. 27 between 3 and 4 s is due also to the 4%/s drop in tunnel stagnation pressure during the run.

During the 0.1-s intervals in which the wire position is fixed, the data can be processed to determine the mean and rms voltage (proportional to mean and rms massflux). The results are shown in Fig. 28. The mean increases from low values near the wall to a maximum at the boundary-layer edge, near 2 mm. The rms fluctuations increase outward from the wall to a peak near the boundary-layer edge where the shear is largest. They then decrease to a near-constant value outside the boundary layer.

Fig. 29 shows spectra obtained from the hot-wire traces at 3 of the 20 positions within the boundary layer. For all 3 spectra, the signal drops rapidly with increasing frequency, as is typical. At 0.58 mm above the wall, the amplitude is lowest, with a few sharp spikes above 50kHz. At 1.58 mm, the overall amplitude is largest, and there is a single peak at about 60 kHz, which may be first-mode instability waves. At 2.98 mm, outside the boundary layer, the amplitude is again lower, with sharp spikes above 60 kHz. The cause of the sharp spikes near the wall and outside the boundary layer is unknown. Wire strain-gauging and probe oscillations remain to be ruled out. Computations of the instability-wave amplifications and frequencies are needed. Although much remains to be done, the results suggest we are already able to measure first-mode waves at Mach 6. Resolving 2nd-mode waves will depend on their frequencies and on the frequency response achievable with the wire and anemometer.

Summary

The Boeing/AFOSR Mach-6 Quiet Tunnel is successfully operating at low cost, but remains quiet only at low Reynolds number. A number of open issues remain regarding the tunnel operation and performance, and achievement of high-Reynolds number quiet flow with simple modifications still appears feasible. The last two designs for the bleed-slot throat provided similar performance, and a thorough polishing of the downstream portion of the nozzle had little effect, so a different cause for the early transition on the nozzle walls is presently being sought. Upstream effects from the shock/boundary-layer interactions in the diffuser are presently a focus of the investigation.

The Hyper2000 remains a geometry that is generic for the forebody of many airbreathing cruise vehicles. Transition is a critical issue for these vehicles, although the mechanisms remain unknown. Measurements suggest that streamwise vortices originating at the leading edge grow rapidly near the compression corners and may cause transition downstream. These vortices can be studied using small roughness elements wrapped around the leading edge. The effect of Reynolds number and roughness height and spacing are presently being determined. These data should help enable development and validation of computational prediction methods, perhaps based on the Görtler instability of the curved streamlines in the sharp corners.

Blunt cones at angle of attack remain a configuration of interest to the user community, yet the mechanisms of transition on these shapes remain uncertain. The existing literature suggests that streamwise instability, roughness, and crossflow can all be important. Measurements of the mechanisms of transition will be required to sort out the dominant effects under different conditions. A new automated traverse for the BAM6QT now enables obtaining a hot-wire profile within a single tunnel run, greatly enhancing productivity of stability measurements. In addition, temperature-sensitive paints are to be used to measure the growth of stationary crossflow waves at angle of attack, although initial measurements have not yet visualized the waves conclusively.

Acknowledgements

The research is funded by AFOSR under grant F49620-00-1-0016, monitored by John Schmisseur, by Sandia National Laboratory, under contract BG-7114, and by NASA Langley, under grant NAG1-02047. Additional support is being provided by a graduate-student fellowship from TRW, and grant NAG-9-1385 from NASA Johnson. Dr. James Kendall, retired from JPL, gave many helpful comments during preparation of the paper.

REFERENCES

[1] Scott A. Berry, Thomas J. Horvath, Brian R. Hollis, Richard A. Thompson, and H. Harris Hamilton II. X-33 hypersonic boundary layer transition. Paper 99-3560, AIAA, June 1999.

[2] H.A. Korejwo and M.S. Holden. Ground test facilities for aerothermal and aero-optical evaluation of hypersonic interceptors. Paper 92-1074, AIAA, February 1992.

[3] AGARD, editor. *Sustained Hypersonic Flight*. AGARD, April 1997. CP-600, vol. 3.

[4] Tony C. Lin, Wallis R. Grabowsky, and Kevin E. Yelmgren. The search for optimum configurations for re-entry vehicles. *J. of Spacecraft and Rockets*, 21(2):142–149, March-April 1984.

[5] I.E. Beckwith and C.G. Miller III. Aerothermodynamics and transition in high-speed wind tunnels at NASA Langley. *Annual Review of Fluid Mechanics*, 22:419–439, 1990.

[6] Steven P. Schneider. Effects of high-speed tunnel noise on laminar-turbulent transition. *Journal of Spacecraft and Rockets*, 38(3):323–333, May–June 2001.

[7] Steven P. Schneider. Flight data for boundary-layer transition at hypersonic and supersonic speeds. *Journal of Spacecraft and Rockets*, 36(1):8–20, 1999.

[8] S. P. Wilkinson, S. G. Anders, and F.-J. Chen. Status of Langley quiet flow facility developments. Paper 94-2498, AIAA, June 1994.

[9] I. Beckwith, T. Creel, F. Chen, and J. Kendall. Freestream noise and transition measurements on a cone in a Mach-3.5 pilot low-disturbance tunnel. Technical Paper 2180, NASA, 1983.

[10] Alan E. Blanchard, Jason T. Lachowicz, and Stephen P. Wilkinson. NASA Langley Mach 6 quiet wind-tunnel performance. *AIAA Journal*, 35(1):23–28, January 1997.

[11] Joseph G. Marvin. Perspective on computational fluid dynamics validation. *AIAA Journal*, 33(10):1778–1787, October 1995.

[12] R.H. Radeztsky, M.S. Reibert, and W.S. Saric. Effect of isolated micron-sized roughness on transition in swept-wing flows. *AIAA J.*, 37(11):1370–1377, November 1999.

[13] Scott Berry, Aaron Auslender, Arthur D. Dilley, and John Calleja. Hypersonic boundary-layer trip development for Hyper-X. Paper 2000-4012, AIAA, August 2000.

[14] Scott Berry, Aaron Auslender, Arthur D. Dilley, and John Calleja. Hypersonic boundary-layer trip development for Hyper-X. *Journal of Spacecraft and Rockets*, 38(6):853–864, Nov.-Dec. 2001.

[15] K. F. Stetson and R. L. Kimmel. Example of second-mode instability dominance at a Mach number of 5.2. *AIAA Journal*, 30(12):2974–2976, December 1992.

[16] P. Balakumar, H. Zhao, and H. Atkins. Stability of hypersonic boundary-layers over a compression corner. Paper 2002-2848, AIAA, June 2002.

[17] S.R. Pate. Supersonic boundary-layer transition: effects of roughness and freestream disturbances. *AIAA Journal*, 9(5):797–803, May 1971.

[18] Jack D. Whitfield and F.A. Iannuzzi. Experiments on roughness effects on cone boundary-layer transition up to Mach 16. *AIAA Journal*, 7(3):465–470, March 1969.

[19] T. Elias and E. Eiswirth. Stability studies of planar transition in supersonic flows. Paper 90-5233, AIAA, October 1990.

[20] Jean M. Delery and A. G. Panaras. Shock-wave/boundary-layer interactions in high-Mach-number flows. In *Hypersonic Experimental and Computational Capability, Improvement and Validation*, pages 2–1 to 2–61. AGARD, May 1996. AR-319 v. I.

[21] W.L. Hankey, Jr and M.S. Holden. Two-dimensional shock wave-boundary layer interactions in high speed flows. AGARDograph 203, AGARD, 1975.

[22] Doyle Knight and Gerard Degrez. Shock-wave/boundary-layer interactions in high-Mach-number flows: A critical survey of current numerical prediction capabilities. In *Hypersonic Experimental and Computational Capability, Improvement and Validation*, pages 1–1 to 1–35. AGARD, December 1998. AR-319 v. II.

[23] Robert Korkegi. Survey of viscous interactions associated with high Mach number flight. *AIAA Journal*, 9(5):771–784, May 1971.

[24] Gary S. Settles and Lori J. Dodson. Supersonic and hypersonic shock/boundary layer interaction database. *AIAA Journal*, 32:1377–1383, July 1994.

[25] J.L. Stollery. Some viscous interactions affecting the design of hypersonic intakes and nozzles. In J.J. Bertin, J. Periaux, and J. Ballman, editors, *Advances in Hypersonics: Defining the Hypersonic Environment*, pages 418–437. Birkhauser, Boston, 1992.

[26] Jean Ginoux. Streamwise vortices in reattaching high-speed flows: a suggested approach. *AIAA Journal*, 9(4):759–760, April 1971.

[27] Luigi de Luca, Gennaro Cardone, Dominique Chevalerie, and Alain Fonteneau. Viscous interaction phenomena in hypersonic wedge flow. *AIAA Journal*, 33(12):2293–2299, December 1995.

[28] K.W. Cassel, A.I. Ruban, and J.D.A. Walker. Separation and instability in the hypersonic boundary layer on a cold wall. Paper 95-2272, AIAA, June 1995.

[29] K.W. Cassel, A.I. Ruban, and J.D.A. Walker. An instability in supersonic boundary-layer flow over a compression ramp. *Journal of Fluid Mechanics*, 300:265–285, 1995.

[30] G. R. Inger. Similitude properties of high-speed laminar and turbulent boundary-layer incipient separation. *AIAA Journal*, 15(5):619–623, May 1977.

[31] F. Grasso, G. Leone, and J.M. Delery. Validation procedure for the analysis of shock-wave/boundary-layer interaction problems. *AIAA Journal*, 32(9):1820–1827, September 1994.

[32] D. H. Rudy, J. L. Thomas, Ajay Kumar, and P. Gnoffo. Computation of laminar hypersonic compression-corner flows. *AIAA Journal*, 29(7):1108–1113, July 1991.

[33] A. Chpoun. Hypersonic flow in a compression corner in 2D and 3D configurations. Paper 89-1876, AIAA, June 1989.

[34] A. Chpoun. Hypersonic flow in a compression corner in 2D configuration. In D. Arnal and R. Michel, editors, *Laminar-Turbulent Transition*, pages 533–543. Springer-Verlag, Berlin, 1990. Proceedings of the IUTAM Symposium, Toulouse, 1989.

[35] G. Simeonides and W. Haase. Experimental and computational investigations of hypersonic flow about compression ramps. *Journal of Fluid Mechanics*, 283:17–42, 1995.

[36] G. Simeonides, W. Haase, and M. Manna. Experimental, analytical, and computational methods applied to hypersonic compression ramp flows. *AIAA Journal*, 32(2):301–310, February 1994.

[37] K.S. Heffner, A. Chpoun, and J.C. Lengrand. Experimental study of transitional axisymmetric shock-boundary layer interactions at Mach 5. Paper 93-3131, AIAA, July 1993.

[38] Frank K. Lu and Kenneth A. Pistone. Preliminary surface pressure measurements of transitional, hypersonic shock boundary layer interactions. Paper 96-4541, AIAA, November 1996.

[39] John E. Lewis, Toshi Kubota, and Lester Lees. Experimental investigation of supersonic laminar, two-dimensional boundary-layer separation in a compression corner with and without cooling. *AIAA Journal*, 6(1):7–14, January 1968.

[40] A.D. Kosinov and S.G. Shevelkov. Experimental investigation of separation and stability of supersonic laminar boundary layers. In *Separated Flows and Jets*, pages 741–745, Berlin, 1990. Springer-Verlag. Proceedings of an IUTAM meeting.

[41] A.A. Maslov, A.N. Shipyluk, A.A. Sidorenko, and Ph. Tran. Study related to hypersonic boundary layer stability on a cone with a flare. Preprint 2-97, Institute of Theoretical and Applied Mechanics, Russian Academy of Sciences, Siberian Branch, Novosibirsk, Russia, 1997.

[42] Charles B. Rumsey and Dorothy B. Lee. Measurements of aerodynamic heat transfer on a 15-deg cone-cylinder-flare configuration in free flight at Mach numbers up to 4.7. Technical Note TN-D-824, NASA, May 1961. Citation 62N71398 in NASA Recon. Supersedes NACA RM L57J10, 1958.

[43] Dorothy B. Lee, Charles B. Rumsey, and Aleck C. Bond. Heat transfer measured in free flight on a slightly blunted 25-deg. cone-cylinder-flare configuration at Mach numbers up to 9.89. RM L58G21, NACA, Sept. 1958. Citation 63N20529 in NASA RECON.

[44] A. Demetriades. Transition in high-speed shear layers. In M. Y. Hussaini and R.G. Voigt, editors, *Instability and Transition, Volume I*, pages 52–67, Berlin, 1990. Springer-Verlag.

[45] F.-P. Liang, Eli Reshotko, and A. Demetriades. A stability study of the developing mixing layer formed by two supersonic laminar streams. *Physics of Fluids*, 8(12):3253–3263, December 1996.

[46] Rudolph A. King, Theodore R. Creel Jr., and Dennis M. Bushnell. Experimental transition investigation of a free-shear layer above a cavity at Mach 3.5. *J. Propulsion*, 7(4):626–634, 1991.

[47] V. DiCristina. Three-dimensional laminar boundary-layer transition on a sharp 8-deg. cone at Mach 10. *AIAA Journal*, 8(5):852–856, May 1970.

[48] John C. Adams, Jr. Three-dimensional laminar boundary-layer analysis of upwash patterns and entrained vortex formation on sharp cones at angle of attack. Technical Report AEDC-TR-71-215, Arnold Engineering Development Center, December 1971.

[49] John B. McDevitt and Jack A. Mellenthin. Upwash patterns on ablating and nonablating cones at hypersonic speeds. Technical Note TN-D-5346, NASA, July 1969.

[50] William L. Oberkampf, Daniel P. Aeschliman, Roger E. Tate, and John F. Henfling. Experimental aerodynamics research on a hypersonic vehicle. Technical Report SAND92-1411, Sandia National Laboratories, Albuquerque, New Mexico, April 1993.

[51] Michael C. Fischer. An experimental investigation of boundary-layer transition on a 10-deg. half-angle cone at Mach 6.9. Technical Report NASA TN-D-5766, NASA, April 1970.

[52] Micheal C. Fischer and David H. Rudy. Effect of angle of attack on boundary-layer transition at Mach 21. *AIAA Journal*, 9(6):1203–1205, June 1971.

[53] George G. Mateer. The effect of angle of attack on boundary-layer transition on cones. *AIAA Journal*, 10(8):1127–1128, August 1972.

[54] George G. Mateer. Effects of wall cooling and angle of attack on boundary-layer transition on sharp cones at Mach 7.4. Technical Report NASA TN-D-6908, NASA, August 1972.

[55] J. Kendall. Wind tunnel experiments relating to supersonic and hypersonic boundary-layer transition. Paper 74-133, AIAA, Jan. 1974.

[56] K.F. Stetson, E.R. Thompson, J.C. Donaldson, and L.G. Siler. Laminar boundary layer stability experiments on a cone at Mach 8, part 3: Sharp cone at angle of attack. Paper 85-0492, AIAA, 1985.

[57] D.E. Boylan, W.T. Strike, and F.L. Shope. A direct comparison of analytical and experimental surface and flow-field data on a 4-deg. cone at incidence in a hypersonic stream with laminar boundary layers. Technical Report AEDC-TR-76-84, AEDC, August 1976. DTIC citation AD-A029367, NASA citation 77N18080.

[58] Martin Simen and Uwe Dallmann. On the instability of hypersonic flow past a pointed cone – comparison of theoretical and experimental results at Mach 8. In *Theoretical and experimental methods in hypersonic flows*. AGARD, May 1992. Paper 31 in CP-514.

[59] A. Hanifi and A. Dahlkild. Stability characteristics of 3-D boundary layer on a yawed cone. In R. Kobayashi, editor, *Laminar-Turbulent Transition*, pages 381–388, Berlin, 1995. Springer-Verlag. Proceedings of the IUTAM Symposium held in Sendai, Japan, September 1994.

[60] Jorgen Olsson. Transition measurements on a sharp cone at angle of attack. Technical Report FFA-TN 1996-16, FFA, the Aeronautical Research Institute of Sweden, 1996.

[61] Jorgen Olsson. Transition measurements on blunt cones at angle of attack. Technical Report FFA-TN 1996-17, FFA, the Aeronautical Research Institute of Sweden, 1996.

[62] Jorgen Olsson. Summary of experimental cone transition research. Technical Report FFA-TN 1996-18, FFA, the Aeronautical Research Institute of Sweden, 1996.

[63] Glen P. Doggett, Ndaona Chokani, and Stephen P. Wilkinson. Effect of angle of attack on hypersonic boundary-layer stability. *AIAA Journal*, 35(3):464–470, March 1997.

[64] Dale W. Ladoon and Steven P. Schneider. Measurements of controlled wave packets at Mach 4 on a cone at angle of attack. Paper 98-0436, AIAA, January 1998.

[65] Dale W. Ladoon. *Wave packets generated by a surface glow discharge on a cone at Mach 4*. PhD thesis, School of Aeronautics and Astronautics, Purdue University, December 1998.

[66] J. Perraud, D. Arnal, L. Dussillols, and F. Thivet. Studies of laminar-turbulent transition in hypersonic boundary layers at ONERA. In *European Symposium on Aerothermodynamics for Space Vehicles, Third*, pages 309–316, November 1998.

[67] K.F. Stetson. Nosetip bluntness effects on cone frustrum boundary layer transition in hypersonic flow. Paper 83-1763, AIAA, July 1983.

[68] K.F. Stetson. Effect of nosetip bluntness on boundary layer transition on the frustrum of a slender cone. AFWAL-TM 82-202-FIMG, Air Force Wright Aeronautical Laboratories, December 1982.

[69] K.F. Stetson. Effects of bluntness and angle of attack on boundary layer transition on cones and biconic configurations. Paper 79-0269, AIAA, January 1979.

[70] M.A. Zanchetta and R. Hillier. Blunt cone transition at hypersonic speeds: the transition reversal regime. In R. Henkes and J. van Ingen, editors, *Transitional Boundary Layers in Aeronautics*, pages 433–440, Amsterdam, 1996. North-Holland.

[71] L.E. Ericsson. Effect of nose bluntness and cone angle on slender-vehicle transition. *AIAA Journal*, 26(10):1168–1174, 1988.

[72] Steven P. Schneider. Hypersonic laminar instability on round cones near zero angle of attack. Paper 2001-0206, AIAA, January 2001.

[73] I. Rosenboom, S. Hein, and U. Dallmann. Influence of nose bluntness on boundary-layer instabilities in hypersonic cone flows. Paper 99-3591, AIAA, June 1999.

[74] D.A. Bountin, A.N. Shiplyuk, and A.A. Sidorenko. Experimental investigations of

disturbance development in the hypersonic boundary layer on a conical model. In H. Fasel and W. Saric, editors, *Laminar-Turbulent Transition. Proceedings of the IUTAM Symposium, Sedona, 1999*, pages 475–480, Berlin, 2000. Springer-Verlag.

[75] A.A. Maslov. Experimental study of stability and transition of hypersonic boundary layer around blunted cone. Technical report, Institute of Theoretical and Applied Mechanics, Russian Academy of Sciences, Siberian Branch, Novosibirsk, Russia, December 2001. Final Technical Report, International Science and Technology Center Grant 1863-2000. Funded by the European Office of Aerospace Research and Development, U.S.A.F.

[76] P. Calvin Stainback. Effect of unit Reynolds number, nose bluntness, angle of attack, and roughness on transition on a 5-deg. half-angle cone at Mach 8. Technical Report NASA TN-D-4961, NASA, January 1969.

[77] J. F. Muir and A. A. Trujillo. Experimental investigation of the effects of nose bluntness, freestream Reynolds number, and angle of attack on cone boundary layer transition at a Mach number of 6. Paper 72-216, AIAA, January 1972.

[78] A. Martellucci, R.S. Neff, and W.H. True III. An experimental investigation of boundary layer transition on a cone at angle of attack. Technical Report TR-69-383, SAMSO, September 1969. Citation AD864331 in DTIC.

[79] Leonidas E. Sakell. *An experimental investigation of boundary layer transition over three axially symmetric bodies at Mach 6.* PhD thesis, New York University, School of Engineering and Science, New York, New York, May 1972. Available from Univ. Microfilms, Order No. 73-9083.

[80] K. F. Stetson. Mach 6 experiments of transition on a cone at angle of attack. *J. of Spacecraft*, 19(5):397–403, September-October 1982.

[81] K.F. Stetson. Hypersonic boundary layer transition experiments. AFWAL-TR 80-3062, Air Force Wright Aeronautical Laboratories, October 1980.

[82] M. S. Holden. Experimental studies of the effects of asymmetric transition on the aerothermal characteristics of hypersonic blunted slender cones. Paper 85-0325, AIAA, January 1985.

[83] M. Holden, D. Bower, and K. Chadwick. Measurements of boundary layer transition on cones at angle of attack for Mach numbers from 11 to 13. Paper 95-2294, AIAA, June 1995.

[84] N. Thyson, A. Todisco, and B. Reeves. Active and passive tripping of frustrum transition at Mach numbers of 8 and 10. Paper 78-1128, AIAA, July 1978.

[85] A. B. Bailey. Effect of boundary-layer transition on center-of-pressure of conical bodies. *AIAA Journal*, 19(8):1082–1083, August 1981.

[86] H.B. Johnson, G.V. Candler, and M.L. Hudson. Numerical study of hypersonic boundary layer transition on a blunt body. Paper 97-0554, AIAA, January 1997.

[87] Eli Reshotko and Anatoli Tumin. The blunt body paradox – a case for transient growth. In H. Fasel and W. Saric, editors, *Laminar-Turbulent Transition. Proceedings of the IUTAM Symposium, Sedona, 1999*, pages 403–408, Berlin, 2000. Springer-Verlag.

[88] S. P. Schneider and C. E. Haven. Quiet-flow Ludwieg tube for high-speed transition research. *AIAA Journal*, 33(4):688–693, April 1995.

[89] Steven P. Schneider, Shin Matsumura, Shann Rufer, Craig Skoch, and Erick Swanson. Progress in the operation of the Boeing/AFOSR Mach-6 quiet tunnel. Paper 2002-3033, AIAA, June 2002.

[90] Steven P. Schneider, Craig Skoch, Shann Rufer, Shin Matsumura, and Erick Swanson. Transition research in the Boeing/AFOSR Mach-6 quiet tunnel. Paper 2002-0302, AIAA, January 2002.

[91] Steven P. Schneider, Shann Rufer, Laura Randall, and Craig Skoch. Shakedown of the Purdue Mach-6 quiet-flow Ludwieg tube. Paper 2001-0457, AIAA, January 2001.

[92] H. Knauss, R. Riedel, and S. Wagner. The shock wind tunnel of Stuttgart university: a

facility for testing hypersonic vehicles. Paper 99-4959, AIAA, November 1999.

[93] Timothy Alcenius, S.P. Schneider, Ivan E. Beckwith, and John J. Korte. Development of square nozzles for high-speed low-disturbance wind tunnels. Paper 94-2578, AIAA, June 1994.

[94] Steven P. Schneider and Craig Skoch. Mean flow and noise measurements in the Purdue Mach-6 quiet-flow Ludwieg tube. Paper 2001-2778, AIAA, June 2001.

[95] Erick Swanson. Mean flow measurements and cone flow visualization at Mach 6. Master's thesis, School of Aeronautics and Astronautics, Purdue University, December 2002.

[96] H. W. Liepmann and A. Roshko. *Elements of Gasdynamics*. John Wiley and Sons, 1957. Republished by Dover, 2002.

[97] Steven P. Schneider, Steven H. Collicott, J.D. Schmisseur, Dale Ladoon, Laura A. Randall, Scott E. Munro, and T.R. Salyer. Laminar-turbulent transition research in the Purdue Mach-4 quiet-flow Ludwieg tube. Paper 96-2191, AIAA, June 1996.

[98] Steven P. Schneider. Initial shakedown of the Purdue Mach-6 quiet-flow Ludwieg tube. Paper 2000-2592, AIAA, June 2000.

[99] I.E. Beckwith, F.-J. Chen, and M.R. Malik. Design and fabrication requirements for low-noise supersonic/hypersonic wind tunnels. Paper 88-0143, AIAA, January 1988.

[100] I.E. Beckwith and B.B. Holley. Görtler vortices and transition in wall boundary layers of two Mach-5 nozzles. Technical Paper 1869, NASA, 1981.

[101] Steven P. Schneider, Shann Rufer, Craig Skoch, Erick Swanson, and Shin Matsumura. Hypersonic transition research in the Boeing/AFOSR Mach-6 quiet tunnel. Paper 2003-XXXX, AIAA, 2003. Submitted to the 2003 AIAA Fluid Dynamics Meeting.

[102] Shin Matsumura and Steven P. Schneider. Development of temperature-sensitive-paint technique for high-speed transition research in the Boeing/AFOSR Mach-6 quiet tunnel. Paper 2003-XXXX, AIAA, 2003. Submitted to the 2003 AIAA Joint Propulsion and Ground Testing Conference.

[103] Shin Matsumura and Steven P. Schneider. Streamwise-vortex instability and transition on a generic scramjet forebody. Paper 2003-XXXX, AIAA, June 2003. Submitted to the June 2003 AIAA Fluid Dynamics Meeting.